Received: 8 March 2021 | Revised: 30 August 2021 | Accepted: 3 September 2021

DOI: 10.1002/wnan.1757

ADVANCED REVIEW

WIREs NANOMEDICINE AND NANOBIOTECHNOLOGY WILEY

Magnetic particle imaging for assessment of cerebral perfusion and ischemia

Peter Ludewig[1] | **Matthias Graeser**[2,3,4,5] | **Nils D. Forkert**[6] | **Florian Thieben**[2,3] | **Javier Rández-Garbayo**[1] | **Johanna Rieckhoff**[1] | **Katrin Lessmann**[1] | **Fynn Förger**[2,3] | **Patryk Szwargulski**[2,3] | **Tim Magnus**[1] | **Tobias Knopp**[2,3]

[1]Department of Neurology, University Medical Center Hamburg-Eppendorf, Hamburg, Germany

[2]Section for Biomedical Imaging at the University Medical Center Hamburg-Eppendorf, Hamburg, Germany

[3]Institute for Biomedical Imaging, Hamburg University of Technology, Hamburg, Germany

[4]Fraunhofer Research Institute for Individualized and Cell-based Medicine, Lübeck, Germany

[5]Institute for Medical Engineering, University of Lübeck, Lübeck, Germany

[6]Department of Radiology and Hotchkiss Brain Institute, University of Calgary, Calgary, Canada

Correspondence
Peter Ludewig, Department of Neurology, University Medical Center Hamburg-Eppendorf, Hamburg, Germany.
Email: pludewig@uke.de

Matthias Graeser, Section for Biomedical Imaging at the University Medical Center Hamburg-Eppendorf, Hamburg, Germany.
Email: ma.graeser@uke.de

Funding information
Bundesministerium für Bildung und Forschung, Grant/Award Number: 13XP5060B; Deutsche Forschungsgemeinschaft, Grant/Award Numbers: GR 5287/2-1, KN 1108/7-1, DFG FOR 2879, LU 1924/1–1: MA 4375/6-1; Forschungszentrums Medizintechnik Hamburg; Gemeinnützige Hertie-Stiftung, Hertie Academy of Clinical Neuroscience; Hermann und Lily Schilling Stiftung

Edited by: Jeff Bulte, Associate Editor and Gregory Lanza, Co-Editor-in-Chief

Abstract

Stroke is one of the leading worldwide causes of death and sustained disability. Rapid and accurate assessment of cerebral perfusion is essential to diagnose and successfully treat stroke patients. Magnetic particle imaging (MPI) is a new technology with the potential to overcome some limitations of established imaging modalities. It is an innovative and radiation-free imaging technique with high sensitivity, specificity, and superior temporal resolution. MPI enables imaging and diagnosis of stroke and other neurological pathologies such as hemorrhage, tumors, and inflammatory processes. MPI scanners also offer the potential for targeted therapies of these diseases. Due to lower field requirements, MPI scanners can be designed as resistive magnets and employed as mobile devices for bedside imaging. With these advantages, MPI could accelerate and improve the diagnosis and treatment of neurological disorders. This review provides a basic introduction to MPI, discusses its current use for stroke imaging, and addresses future applications, including the potential for clinical implementation.

This article is categorized under:

Diagnostic Tools > In Vivo Nanodiagnostics and Imaging

Therapeutic Approaches and Drug Discovery > Nanomedicine for Neurological Disease

Peter Ludewig, Matthias Graeser, Nils D. Forkert, Tim Magnus, and Tobias Knopp contributed equally to this study.

KEYWORDS
imaging, magnetic particle imaging, stroke, theranostics

1 | INTRODUCTION

Imaging techniques are indispensable for the diagnosis and treatment of ischemic stroke and other neurological disorders. In addition to ruling out hemorrhages and other neurological diseases mimicking acute ischemic stroke symptoms, a major objective of imaging patients with an acute ischemic stroke is determining the volume, location of the infarct core, and the surrounding ischemic penumbra (Baird et al., 1997). Physiologically, a cerebral artery occlusion does not lead to an immediate, irreversible injury of corresponding brain regions due to a reduced blood supply by collateral vessels such as the circle of Willis or leptomeningeal collaterals. Following these physiological considerations, the infarct core is defined as the irreversibly damaged tissue. In contrast, the hypoperfused brain tissue within the penumbra is dysfunctional and at an increased risk of necrosis but still salvageable and represents the target for any treatment approach. Patients with a small core and a large penumbra are likely to benefit most from any intervention (e.g., thrombectomy and thrombolysis). Thus, the ratio of the stroke core and penumbra volume is often used for treatment selection. Unfortunately, the infarct core expands into the penumbra over time in a dynamic process. This observation has led to the concept of "time is brain" for treating acute ischemic stroke patients, postulating that a faster recanalization of the occluded artery leads to more preserved tissue and an improved clinical outcome. So, any image-based diagnosis needs to be quick (Saver, 2006).

PET studies revealed that salvageable tissue exists for up to 24 h. Consistent with these findings, more and more studies show that patients might benefit from thrombectomy even after more than 12 h. Therefore, treatment decision-making in acute ischemic stroke patients is increasingly based on imaging information in addition to clinical criteria, including the time window. Stroke therapy is becoming more and more personalized medicine. Thus, more precise imaging is needed to identify with greater accuracy those patients who benefit from therapy in an extended time window. However, the low temporal resolution, greater than 1 s, in standard CT and MRI perfusion imaging can have a significant effect on the quantified infarct core and penumbra segmentations, depending on the quantification method. This variation can deprive patients of optimal stroke treatment. Magnetic Particle Imaging (MPI) is a tomographic imaging technique with a high temporal resolution of up to 46 frames per second in 3D(+t) datasets (or even more than 1000 frames per second in 2D(+t) datasets). MPI may enable faster, more reliable, and more accurate identification of the infarct core and penumbra and subsequently improve prediction of which patients will benefit from stroke treatment. This review will highlight the first preclinical stroke imaging studies and the recent progress in the development of MPI scanners for humans.

2 | MAGNETIC PARTICLE IMAGING

The physical principle of MPI relies on the non-linear shape of the particle magnetization curve (Gleich & Weizenecker, 2005). When the particles are excited by an oscillating magnetic field, the magnetization behavior acts as a non-linear mixer of all applied fields (Rahmer et al., 2009). If the magnetization response is recorded using inductive sensors, the induced signal shows higher harmonics and, in the case of multidimensional excitation, mixing of all excitation frequencies. As the shape of the excitation field is typically purely sinusoidal, the presence of these higher frequency components already encodes the presence of tracer material within the field of view (FOV). To ensure a spatial encoding, a linear gradient, the so-called selection field, is applied featuring a low field region in its center. This region can have the shape of a line (referred to as field-free line, FFL) or a point (referred to as field-free point, FFP) depending on the field generator topology (Weizenecker et al., 2008). The superposition of the two fields results in a unique field vector sequence at every point in space. In consequence, the magnetization time sequence in this spatial position is unique as well. Under the assumption that the particle response is linearly dependent on its concentration, which holds true for most tracer systems at clinically relevant concentrations, the imaging problem can be described as a linear system of equations (Grüttner et al., 2013; Lu et al., 2013), which can be solved using iterative linear solvers (Knopp et al., 2010). The basic principle of signal generation, spatial encoding, and reconstruction is shown in Figure 1.

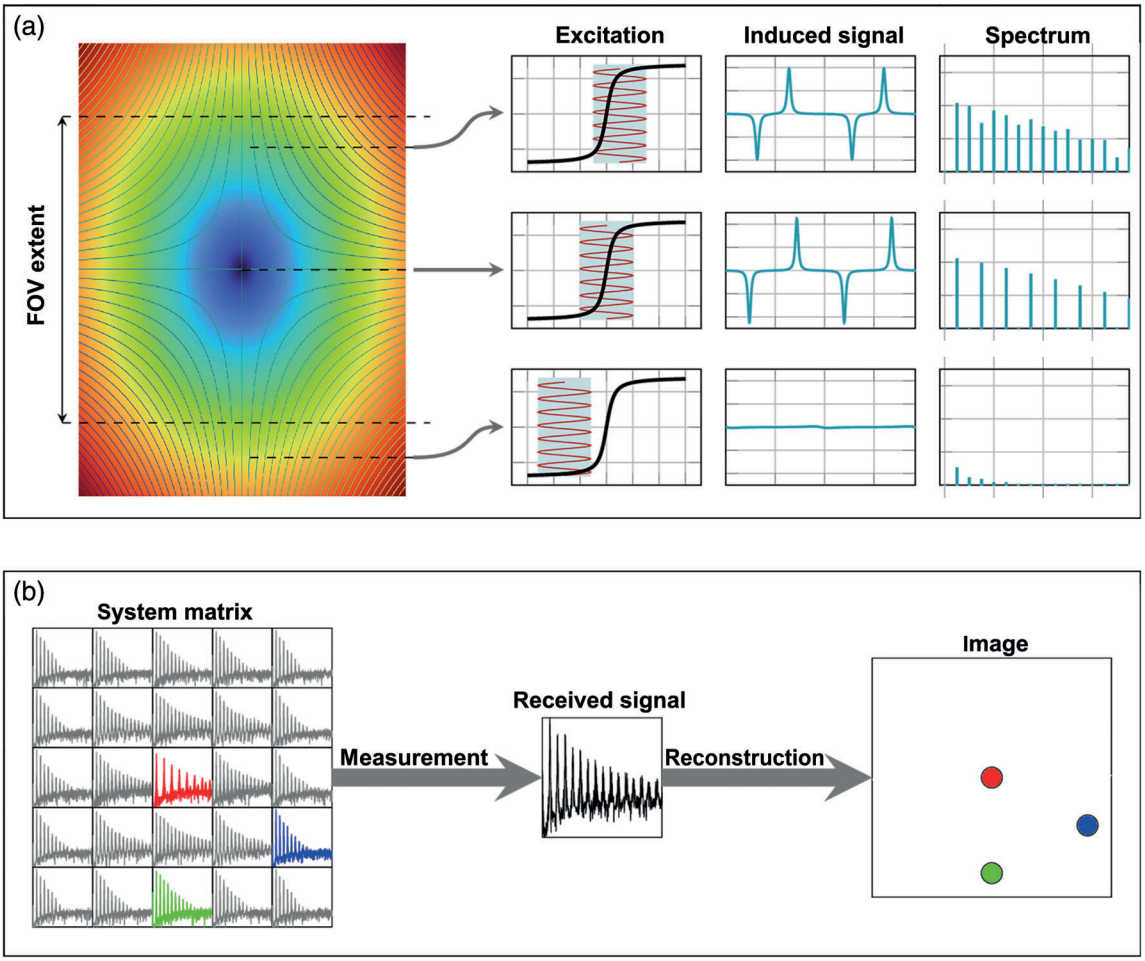

FIGURE 1 Fundamental principles of MPI. MPI images the distribution of nanoparticles within a defined FOV. In the example, a 1D sinusoidal excitation field is applied (a). In superposition with a gradient field seen on the left side, the excitation field moves the low field region over space in time, defining the field of view (FOV). Tracer distributions within the FOV experience a changing magnetization causing signals in receive coils nearby. As the selection field is unique in strength and orientation throughout the FOV, the field sequence and, therefore, the signal response is also unique. This can be directly seen in the signal spectrum on the right side, which acts as a local fingerprint encoding a specific position in space (b). The image reconstruction shown on the bottom uses this fingerprint and determines the spatial distribution by solving a linear system of equations

The imaging performance is mainly determined by the instrumentation and the magnetization properties of the tracers. The spatial resolution of the MPI is driven by a combination of the slope of the dynamic magnetization curve on the one hand and the gradient strength of the encoding field on the other hand (Gleich & Weizenecker, 2005). Another parameter affected by the tracer and the instrumentation is the sensitivity (Knopp et al., 2011). Similar to the spatial resolution, steep magnetization curves provide good sensitivity. The sensitivity is influenced mainly by the coil and amplifier noise on the instrumentation side, as patient noise dominance is hard to achieve below 500 kHz (Schmale et al., 2010). The temporal resolution is mainly dependent on the instrumentation, namely on the selection of the drive field frequencies. In multidimensional excitation systems, these frequencies need to be chosen in a way that they are dividers of a common base frequency (Knopp et al., 2008). The greatest common divisor of those frequencies defines the repetition frequency and, therefore, the frame rate. However, when designing the system, the chosen frequencies also impact the signal induction, the dynamic magnetization curve, and the demands on the hardware. Therefore, a compromise between speed, hardware efforts, and particle dynamics needs to be found. An overview of the history of different scanner developments can be seen in Figure 2.

One of the main advantages of MPI is the capability to image fast dynamic processes within the body. In preclinical systems, MPI can reach a frame rate of up to 1050 frames per second (Vogel et al., 2020), which allows MPI to capture even fast dynamic movements like blood flow within the aortic arch. As the aortic arch is the region of the most rapid

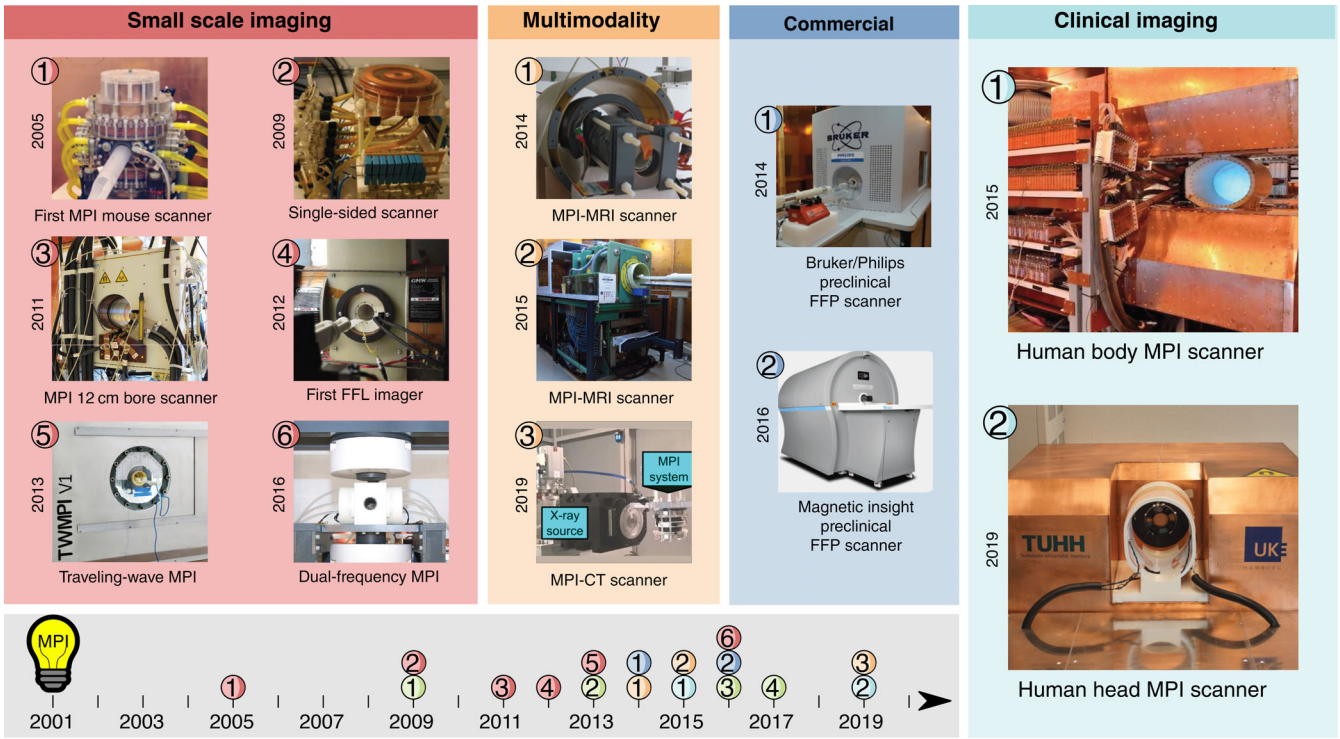

FIGURE 2 History of MPI. After invention in 2001, Bernhard Gleich and Jürgen Weizenecker presented the first small animal MPI scanner (Gleich & Weizenecker, 2005). After that, several groups worked on different field geometries (Draack et al., 2021; Goodwill et al., 2012; Sattel et al., 2009; Vogel, Rückert, et al., 2014), upscaling (Gleich et al., 2010), and multimodal solutions (Franke et al., 2016; Vogel, Lother, et al., 2014; Vogel, Markert, et al., 2019). In 2014 and 2016, the first two commercial small animal imaging units were introduced by Bruker BioSpin and magnetic insight. The first two scanners suitable for clinical use were presented in 2015 by the Philips research group (Rahmer et al., 2018) and 2019 by the University Medical Center Hamburg (Graeser et al., 2019)

velocities within the human body, MPI proves to be capable of imaging any important physiological dynamic without the need for triggering techniques or multiple tracer injections. The imaging speed is mostly determined by the chosen excitation frequencies as well as the trajectory density. It is independent of the bore size, which makes such high speeds possible in human-scale systems. If a specific measurement protocol does not provide enough imaging speed, a preprocessing step before image reconstruction allows reconstructing processes that are repetitive in nature using reordering of the raw data. Thus, artifact-free imaging without triggering is even possible for low imaging speeds (Gdaniec et al., 2020). The spatial resolution can reach down to 330 μm (Vogel, Markert, et al., 2019; Vogel, Rückert, et al., 2019), while most systems have resolutions in the range of 1–2 mm (T. Knopp et al., 2017). As a gradient strength of about 2–3 T/m/μ0, which is used in preclinical scanners, is also feasible for human-scale scanners, a similar resolution is possible in human applications (Rahmer et al., 2018). The sensitivity of MPI systems currently reaches down to about 900 pg iron content using optimized receive coils and electronics commercially available tracer material (Graeser et al., 2017, 2020). This allows long-time continuous imaging over several days without iron overdose. The high sensitivity also enables cell tracking for a very low number of cells, probably down to 1–10 cells (Graeser et al., 2020; Zheng et al., 2015), providing more possibilities for stem cell research.

As described above, the imaging process relies on the dynamic magnetization curve of the tracer material. This dynamic process relies on several parameters, including the physical parameters of the tracer like the base material, crystal structure, shape, and the coating size and material (Rauwerdink et al., 2009; Rauwerdink & Weaver, 2010a, 2010b; Weaver et al., 2009); (Graeser, Bente, & Buzug, 2015; Graeser, Bente, Neumann, & Buzug, 2015; Viereck et al., 2017). Additionally, the local microenvironment of the tracer influences the magnetization behavior, for example, the temperature of the medium or the viscosity. In multicontrast (or multicolor) MPI, this dependency is exploited to use the tracer as a microsensor and encode these physiological parameters within the image domain (Haegele, Panagiotopoulos, et al., 2016; Möddel et al., 2018, 2020; Rahmer et al., 2015; Shasha et al., 2019; Stehning et al., 2016; Szwargulski et al., 2019; Szwargulski et al., 2020; Utkur et al., 2019). Figure 3 outlines different possibilities of multicontrast MPI.

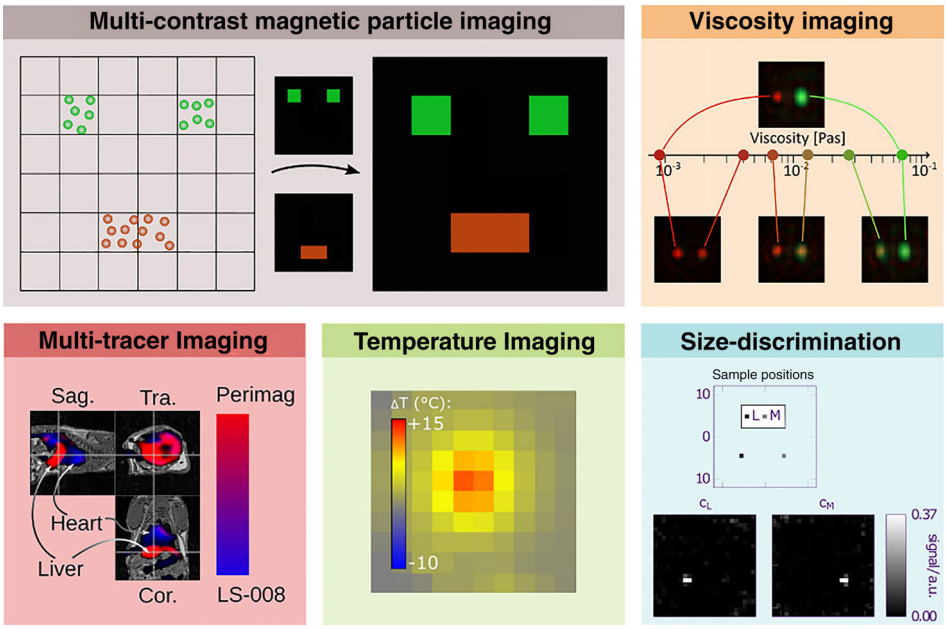

FIGURE 3 Application fields of multicontrast MPI. Multicontrast MPI (top left) allows the determination of additional parameters like the viscosity (Möddel et al., 2018) (top right) or the temperature (Salamon et al., 2020) (bottom middle). Alternatively, multicontrast MPI can also be used to image multiple tracers simultaneously (Szwargulski et al., 2018) (bottom left) or even to determine the size of multiple tracer systems (Shasha et al., 2019)

Most of the scientific research in MPI currently focuses on the preclinical side as only a few imaging systems with a human-sized bore exist. When scaling up MPI systems, new challenges arise both on the physiological and technological sides. The main technical challenges are a quadratic rise of the power consumption for all field generators and a rising voltage of the drive field coils caused by higher currents and larger inductance due to larger coil diameters.

Considering the imaging performance of human-scale systems, a larger diameter results in weaker coupling of the receiver coils with the tracer magnetization. This leads to a lower sensitivity which roughly scales with the diameter if a coil noise dominance is assumed. Due to the increased tracer dosage compared with rodents, this effect is compensated for most applications. Recent developments using optimized receive coils and receive electronics showed rapid improvement of the achieved sensitivity, which will also impact the sensitivity of human-sized systems (Graeser et al., 2017, 2020; Zheng et al., 2015).

The third impact of upscaling is physiological limits, namely the peripheral nerve stimulation (PNS) and the tissue's specific absorption rate (SAR). The oscillating magnetic fields induce eddy currents in human tissue, which can excite peripheral nerves at low drive field frequencies. At higher frequencies, the SAR dictates a lower limit than PNS (Saritas et al., 2015, 2013). A PNS and SAR study by Schmale et al. (Saritas et al., 2013; Schmale et al., 2015) showed that for human torso scale systems, the PNS limit is roughly around 3 mT. As these scales down the FOV, low-frequency focus fields are introduced, which consequently cover a larger region with patches of these smaller FOVs. The drive field frequency can be shifted to a higher region until SAR limits become dominant to recover the high temporal resolution.

In summary, the upscaling faces three opposing requirements that determine the complexity of the imager. The first is imaging performance parameters like the temporal and spatial resolution and the sensitivity. Different medical applications need a distinct focus on these imaging parameters, while a “one fits all” machine needs to cover all parameters at once. The second requirement is physiological and electrical limits that need to be met to ensure the safety of the patient and the operator. These cannot be overcome and also have to apply for medical regulation standards. The third one is the technological complexity of the system. As described above, the “one fits all” machine may be advantageous as it provides the physician a variety of imaging possibilities and raises the hardware side's effort to its limits. Besides rising costs, this leads to a spatially fixed system with high room infrastructure and space demands.

Up to now, two human-sized MPI systems were presented, one capable of torso imaging and the other intended for brain imaging. The first one was presented by Rahmer et al., 2018.

This system was aimed as a "one fits all" machine featuring a bore fitting a human torso. It provided a selection field of 2.8 T/m/μ_0 resulting in an expected resolution of around 1 mm (Bontus et al., 2015). The drive field frequency was chosen to be 150 kHz with 3 mT/μ_0 field strength resulting in a frame rate of 568 volumes per second (Rahmer et al., 2018). To cover a large FOV, the system provided focus fields of 8 mT, which makes the system the most flexible until today. On the other hand, the system had comparable infrastructural needs as an MRI tomograph being permanently installed and a large infrastructure room.

The second human-scale MPI system is a brain scanner developed to perform surveillance imaging directly on the stroke or intensive care unit (see Figure 4; Graeser et al., 2019). The aim of this head scanner is a specialized system that provides the imaging parameters needed for monitoring applications but reduces the technical effort to a minimum using a low-field approach. The system currently provides a selection field of only 0.25 T/m/μ_0 with a drive field frequency of 25 kHz and 6 mT/μ_0 excitation field strength. With these parameters, the system is capable of reaching a sensitivity limit of 263 pmol/L_{Fe} with a frame rate of 2 Hz and a spatial resolution of 5 mm. The clear advantage of the low-field approach is its small footprint of roughly 1 m^2 and the capability of working on a standard 230 V power plug. In addition, the system is self-shielded and does not need any further infrastructure as cooling or radiofrequency shields.

Another, yet not finished, demonstrator is built at the St. Martinos Center for Biomedical Imaging. The aim is to develop a human-sized functional magnetic particle imaging system and exploit the potential 40 times higher contrast to noise ratio of MPI (Cooley et al., 2018; Mason et al., 2017).

As a tracer-based imaging modality, the reconstructed images provide no anatomical reference and are, therefore, sometimes hard to judge. To overcome this challenge, several systems have been developed on a preclinical scale to combine MPI with anatomical imaging modalities like MRI or CT (Franke et al., 2016, 2020; Vogel, Lother, et al., 2014; Vogel, Markert, et al., 2019; Vogel, Rückert, et al., 2014). Due to the fast imaging speed, MPI can also be combined with optical coherence tomography (OCT) to provide intravenous tracer tracking and use this information to incorporate prior knowledge for the OCT image reconstruction (Griese et al., 2019; Latus et al., 2019).

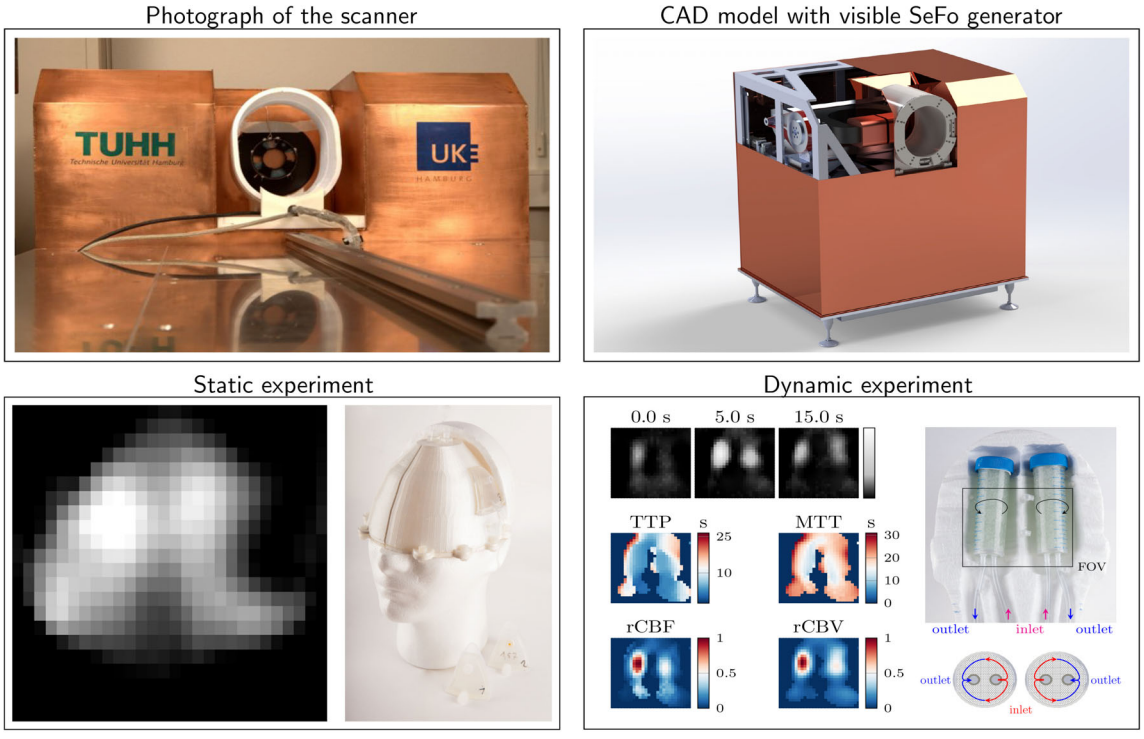

FIGURE 4 Overview of the neurological MPI scanner. The selection field generator (SeFo) is placed under a copper shield. It can be seen in the cutout on the CAD model of the scanner. The working scanner can be seen in the scanner photo. In a static experiment, a human-sized phantom was filled with an effective iron concentration of 965 ng/mL Fe. A small region on the side was left empty to simulate a stroke of 42 mL. The stroke region is visible on the right side of the reconstruction. The capability to generate perfusion maps is shown on the right side, where a phantom filled with glass spheres was perfused with water. With a bolus injection of tracer, the perfusion parameters were calculated and visualized in parameter maps. Reprinted with permission from Graeser et al. (2019)

The development of human-scale MPI systems is still in its beginnings. One research field is the optimization of the field generator, especially the section field generator. The selection field strength can still be improved with power optimization techniques and effective iron field guide design. As this strength is directly coupled to the spatial image resolution, the currently achieved image resolution does not represent the physical limit for MPI. For large volumes, the improvement in tracer performance can be translated into larger scan volumes by reducing the gradient. As different groups contributed to scientific achievements over the past years with different technological foci, the true potential of MPI lies in combining these features into one machine.

3 | TRACER MATERIAL FOR MAGNETIC PARTICLE IMAGING

As a tracer-based imaging modality, the entire imaging performance inherently depends on the scanner instrumentation and the tracer characteristics. Therefore, intensive research on the optimal MPI tracer has been carried out in the past decade, leading to various approaches for optimizing image quality.

The research can be divided into two areas: optimizing the tracer core to improve the MPI performance regarding its spatial resolution and sensitivity and functionalizing the tracer surface to target specific medical applications.

Tracers in MPI consist of a magnetic core, which defines the magnetic properties, and a non-magnetic coating with two main functions: First, it prevents agglomeration, and, second, it defines its physiological properties. The core is usually made of magnetite (Fe_3O_4) with a high magnetic moment of $4.1\mu_B$, where, μ_B is the Bohr magneton (Petrov & Ustinov, 2010).

In the early years of MPI, ferucarbotran (Resovist), a clinically approved tracer with a magnetite core, was commonly used. Later, other commercially available tracers like Perimag (and VivoTrax) based on ferucarbotran and maghemite nanoflowers (γ-Fe_2O_3) like Synomag showed their potential in MPI. Figure 5 compares Resovist (batch: 81049S), Perimag (lot: 05617102-05), and Synomag (lot: 08219104-03) in a magnetic particle spectroscopy (MPS)

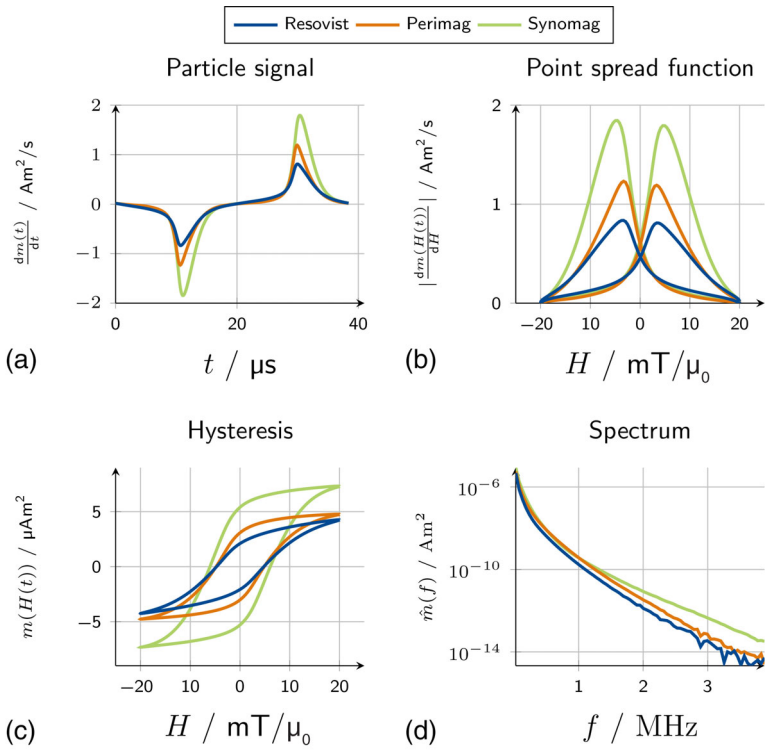

FIGURE 5 Comparison of MPI tracers. The figure shows MPS measurements comparing Resovist (black), Perimag (blue), and Synomag (orange) with an iron amount of 56 µg in a 15 µL (66.6 mmol/L) solution. The derivative of the magnetic moment is shown for one excitation period in (a) and as a point spread function depending in (b). The later plot also shows the phase lag of the particle signal, which can be seen in the peaks being shifted to zero-field strength. The magnetic moment is additionally shown in the hysteresis plot as a function depending on the magnetic field (c) and in the Fourier domain as frequency spectra of the odd harmonics (d)

experiment, which is an established method for determining the MPI imaging performance with a 1D field excitation without spatial encoding (Biederer et al., 2009). The three samples contained an iron amount of 56 μg in 15 μL resulting in an iron concentration of 66.6 mmol/L. Using a custom-made and calibrated MPS, they were exposed to a magnetic field amplitude of 20 mT/μ_0 at 26 kHz. The measurements revealed an average amplification factor of 1.5 between Perimag compared with Resovist and 2.2 between Synomag and Resovist, which directly translates into an increase in sensitivity when using the tracer, providing a higher MPI signal.

Tracer research needs to deal with two conflicting goals regarding imaging performance. It is known that if the saturation field strength is the lower, the larger the particle cores are. It implies that the spatial resolution in MPI improves with increasing particle volume. However, its inertia and anisotropy depend on the particle size, especially on the nonmagnetic shell, resulting in the particle relaxation effects and turn decreasing signal and resolution if the size gets too large.

Finding the optimal particle size and shape is thus one of the core questions in tracer research done both experimentally and in simulation studies. The influence of the diameter of several monodisperse particles on the MPS signal intensity was compared with determine the optimal size for MPI (Ferguson et al., 2013). Tracer with a median diameter of 20 nm and hydrodynamic diameter equal to 30 nm showed the best performance.

Size separation due to forced magnetic field (Arsalani et al., 2021) and centrifugation (Dadfar et al., 2020) is an additional way to increase the MPI signal intensity. In simulation studies, magnetic nanoparticle chains with a specific length improve signal intensity (Zhao & Rinaldi, 2020). In addition to spherical particles and particle chains, maghemite nanoflowers (Fe_2O_3) (Bender et al., 2018; Karpavičius et al., 2021) provided an excellent MPI performance with a fourfold higher signal than Resovist (Szwargulski et al., 2020). Other authors reported even higher amplification factors (Ziemian et al., 2018), where the signal was a factor of 6.6 higher than Resovist, resulting in improved spatial resolution in imaging experiments. Regarding the particle shape, recently, cubic iron oxide nanoparticles with more than a threefold MPI signal increase compared with VivoTrax were presented (Wang et al., 2020).

Synthesizing multicore nanoparticles can result in a fourfold signal increase compared with Resovist in MPS measurements (Kratz et al., 2018). In vivo angiography of inferior vena cava and aorta of rats with these particles shows the potential of MPI for quantitative assessment of the vascular anatomy (Mohtashamdolatshahi et al., 2020). In another effort, carbon-coated FeCo nanoparticles were presented by Song et al. (2020), revealing a sixfold higher MPI signal than VivoTrax, which has a similar performance as Resovist. In summary, recent progress in particle synthesis has shown that different approaches can increase the particle signal by a factor of 3–6 compared with the gold standard Resovist. It is an important future research topic whether combining the different approaches achieves even higher signals.

Moreover, modification of the particle surface to improve imaging quality has made rapid progress within the last decade. A large class of MPI tracers, including the clinically used tracer Resovist (Reimer & Balzer, 2003), have a coating based on a glucose molecule like dextran or carboxydextran. After intravenous injection, the tracer remains in the blood pool for a short time and is then continuously taken up by the Kupffer cells in the liver and spleen (Guzy et al., 2020; Hamm et al., 1994). While this is helpful for liver applications, it shortens the time window for other applications such as perfusion studies. Typical half-life times of these tracers are about 6 min in human blood (Hamm et al., 1994) and about 5 days in the liver of rats (Lawaczeck et al., 1997). Because of this, there is great interest in increasing the half-life time of MPI tracers and ideally developing tracers that remain in the blood pool for a longer time, thus allowing image vessels and organ perfusion over a long period.

Two different approaches have successfully reached this goal: Initial experiments (Khandhar et al., 2015) attempted to increase the blood half-life time by tuning the surface coating with polyethylene glycol (PEG). MPS experiments in mice revealed a blood half-life time of 19 min. These PEG-coated particles were further improved (Khandhar et al., 2017), with a blood half-life of about 105 min in mice studies. The biodistribution of these particles was tracked in short-term experiments and long-term clearance (Keselman et al., 2017), showing a blood half-life time of 4.2 h, 6.5 days in the liver, and 18.2 days in the spleen of rats. With the 3.4-fold better MPI signal of LS-008 compared with Resovist MPI, in vivo angiography was performed in mice studies showing the potential of real-time perfusion imaging (Kaul et al., 2017). Furthermore, due to the increased MPI signal intensity of LS-008, the spatial resolution improved to 330 μm (Vogel, Rückert, et al., 2019), and the extended blood half-life time allows for perfusion imaging (Kaul et al., 2017). Synomag-D, another PEG-coated tracer with a blood half-life time of 60 min, was used to monitor in vivo intracranial cerebral hemorrhage in mice (Szwargulski et al., 2020).

An alternative approach to adjusting the particle surface for increasing the blood half-life time is to load red blood cells (RBCs) with particles. Practically, the blood retention time was increased with Resovist-loaded RBCs to about

14 days compared with bulk Resovist with a typical retention time of about 1 h in mouse bloodstream (Antonelli et al., 2016). Further MPS experiments with Perimag and Synomag in human RBCs showed a promising potential of Perimag-COOH-loaded RBCs for MPI (Antonelli et al., 2020).

In addition to increasing the half-life time of magnetic nanoparticles, there has also been intensive research in the direction of functionalizing tracers so that specific cells or regions are targeted. These functionalized nanoparticles showed a promising potential in multimodal imaging, both in MPI and MRI (Erathodiyil & Ying, 2011; Hola et al., 2015; Liu et al., 2010).

The tracking and monitoring of ferumoxytol-labeled mesenchymal stem cells (MSCs) was performed with MPI, imaging the total MPI signal decline in vivo within 12 days (Sehl et al., 2020). Later a method for ex vivo counting of cells was presented (Sehl et al., 2020). Bone MSCs labeled with cubic iron oxide nanoparticles were used for stem cell tracking, monitoring the amount and location of the cells over 9 days (Wang et al., 2020). MPI showed to be capable of performing target drug delivery using a peptide CREKA in a mouse breast cancer model (Du et al., 2019). By loading chylomicrons with iron oxide nanoparticles, the in vivo lipoprotein uptake in brown adipose tissue of mice can be quantified using MPI (Hildebrand et al., 2020). In the field of therapeutic imaging, MPI can be used for monitoring the application of hyperthermia. Recently, the combination of targeted drug delivery with nanoparticles and the application of hyperthermia while monitoring the particle location with MPI could be shown (Chandrasekharan et al., 2020; Dadfar et al., 2020; Du et al., 2019; Song et al., 2020).

The toxicity of the tracer materials is a topic that needs addressing. Challenges for clinical translation arise from missing regulatory-approved MPI- specific tracers. Existing SPIOs, developed for other applications, were repurposed for off-label MPI use. Tracers such as ferucarbotran showed minor side effects similar (Onishi et al., 2009).

Compared with gadolinium, MPI tracers have the advantage of being biodegradable, whereas concerns have emerged due to cerebral gadolinium deposits in patients after repetitive applications (Kanda et al., 2014). In contrast to gadolinium, most preclinical trials found a steady decrease in the tracer signal and complete removal or degradation of the SPIOs from the brain parenchyma (Ludewig et al., 2017; Szwargulski et al., 2020). These studies suggest that SPIOs get phagocytosed and digested by macrophages or microglia, followed by incorporating the degraded iron into hemoglobin, which others observed (Bulte, 2019). In the trials mentioned above, no mortality after tracer injections was observed in stroke and bleeding, and the tracer did not increase stroke or bleeding sizes.

In porcine brains, no iron deposition in the brain was observed 9–12 months after intravenous infusion of ferumoxytol (Theruvath et al., 2020). A case–control study found no significant signal differences in brain MRI of children and young adults after exposure to ferumoxytol compared with unexposed children (Iv et al., 2020). Nevertheless, it is necessary to investigate whether SPIOs get entirely removed from the brain parenchyma or increase neurotoxicity when the blood–brain barrier collapses.

One primary clinical concern in imaging techniques regards the risk of immediate hypersensitive reactions after intravenous infusion of contrast agents. Iodine-based contrast agents used for CT scans are long known for risk of acute reactions with approximately 4%–12% for the use of ionic contrast agents and 1%–3% for non-ionic contrast mediums (Bush & Swanson, 1991). The risk of severe and potentially life-threatening events was 0.2% and 0.04%, respectively, leading to the predominating use of non-ionic agents (Bush & Swanson, 1991; Cochran, 2005). On the other hand, gadolinium-based contrast agents show a shallow risk of hypersensitive effects with an overall rate of 0.09% of immediate reactions and 0.005% risk of severe effects (Behzadi et al., 2018).

Safety data drawn from the phase I–III trials of ferucarbotran reported one anaphylactic reaction in 1053 doses (0.09%) and 75 possibly, probably, or definitive drug-related adverse effects, with a majority considered as mild symptoms (Reimer & Balzer, 2003).

Ferumoxytol, another SPIO with an FDA approval for the treatment of iron deficiency anemia, was provided with an FDA boxed warning in 2015 due to the occurrence of 79 anaphylactic reactions, 18 of which had been fatal despite instant medical treatment (US Food and Drug Administration, 2015).

However, approximately 1.2 million doses of ferumoxytol have been administered since the FDA approval in 2009 and the warning release in 2015 (Vasanawala et al., 2016). Four randomized and one non-randomized study reported severe anaphylactic reactions ranging from 0.02% (2/8666 patients) to 1.3% (1 /80 patients). Combined, these studies report a 0,046% rate of severe anaphylactic reactions (5/10,575 patients), whereas the majority of all reported adverse effects was considered mild (Adkinson et al., 2018; Hetzel et al., 2014; Macdougall et al., 2014; Schiller et al., 2014; Vadhan-Raj et al., 2014). A multicenter safety analysis based on a non-randomized observational database of off-label use of ferumoxytol in MRI studies reported no severe or fatal adverse effects in 3215 patients (Nguyen et al., 2019).

Taken together, though not as rare as in gadolinium-based agents, the risk of severe anaphylactic reactions in SPIOs is rare and slightly lower than in iodine-based agents. It can be further reduced by administering the agents in clinical settings with trained personnel, emergency equipment, and cardiovascular monitoring during and after the application.

4 | IMAGING OF NEUROLOGICAL DISORDERS

4.1 | Potential use of MPI in acute ischemic stroke management

Up to now, multiparametric MRI and CT perfusion (CTP) imaging are the primary modalities for determining the infarct core and penumbra and are commonly used for the image-based acute ischemic stroke treatment decision. Perfusion-weighted MRI (PWI) and CTP are contrast-based imaging techniques (gadolinium and iodine, respectively), which acquire a temporal series of 3D images with a temporal resolution of 1.0–2.5 s of the brain after administration of the exogenous contrast agent. The resulting images display the contrast agent's spatio-temporal (4D) dynamics with reduced and delayed perfusion of the ischemic brain tissue. Due to the high dimensionality and complexity of the 4D image sequences, the PWI or CTP datasets are typically not assessed directly but used to calculate perfusion parameter maps, which are necessary to define the infarct core and the penumbra of the acute ischemic stroke using a wide range of suggested thresholds (Forkert et al., 2013). More precisely, the 4D datasets are used to compute voxel-wise perfusion parameters in the brain, including cerebral blood flow (CBF), cerebral blood volume (CBV), mean transit time (MTT), and the time to the maximum of contrast accumulation ($T_{\max}$).

Two main techniques to acquire perfusion-weighted MRI datasets are dynamic susceptibility contrast (DSC) MRI and dynamic contrast-enhanced (DCE) MRI. Briefly described, DCE sequences take advantage of the T1 contrast, while DSC techniques utilize susceptibility effects arising from the application of paramagnetic contrast agents. DCE MRI is sensitive to extravasation effects enabling calculation of the vascular permeability as an additional parameter based on the concentration-time curves. However, since vascular permeability is not used clinically for acute ischemic stroke treatment decision making and T2* effects are considerably stronger than T1 effects, DSC perfusion imaging is the most frequently employed technique for imaging acute stroke patients. Briefly described, DSC measures the susceptibility effects resulting in a T2* shortening of the proton spin relaxation times as the contrast agent bolus travels through the brain.

CT perfusion sequences measure the spatiotemporal changes in density caused by the contrast agent while flowing through the brain. A benefit of CTP compared with DSC is that the contrast concentration is linearly related to the attenuation measured in CT so that no complex correction formulas are needed to transform the measured signal curves to concentration–time curves. The relative or absolute concentration-time curves measured by CTP and DSC-PWI cannot be used directly to determine the perfusion parameters of interest. The measured concentration–time curves are affected by the patient-specific cardiac output function and the contrast agent injection protocol. To correct for these effects, each tissue concentration–time curve is typically deconvolved with the arterial input function (AIF), which is usually identified manually or automatically at the contralateral internal carotid artery or middle cerebral artery before calculating perfusion parameter maps (Winder et al., 2020). While several techniques have been proposed to solve the ill-posed deconvolution problem, the block-circulant singular value decomposition is probably the most often used approach for this purpose (Wu et al., 2003). After deconvolution, the perfusion parameters described above can be determined from the resulting residue curve of each voxel. For example, CBF can be determined by the slope of this curve, MTT by the full-width-half-maximum, CBV by the area under this curve, and $T_{\max}$ by identifying the time point with the maximum value in the residual curve (Forkert et al., 2014). Slightly different definitions of these parameters have been proposed. After this, the hypoperfused tissue is typically segmented using a global threshold greater than 6 s, while the ischemic core can, for example, be determined using a relative CBF threshold of less than 30% compared with the contralateral hemisphere (Campbell et al., 2011). The volumetric difference between the ischemic core and the hypoperfused tissue is typically assumed to be the tissue-at-risk.

DSC-PWI and CTP both have their benefits and limitations when comparing each other. First, it needs to be highlighted that both techniques use exogenous contrast agents that have been suggested to be potentially harmful to patients in recent studies, for example, showing gadolinium deposition in the brain and other organs with unknown long-term effects (Guo et al., 2018; see chapter 3). DSC-PWI has a much better signal-to-noise ratio (SNR) than CTP, which usually leads to smoother-looking perfusion parameter maps and better segmentation of the hypoperfused tissue. In contrast, considerably more spatial and temporal smoothing is needed to achieve similar results using CTP datasets.

However, excessive smoothing can also bias the absolute perfusion parameter calculation. On the other hand, CT scanners are much more widely available in the emergency room setting, allowing faster image acquisition, which is essential given the time constraints of acute ischemic stroke diagnosis ("time is brain"). Furthermore, CT scanners are also significantly cheaper than MRI scanners, so that they are more widely available in small and rural hospitals. While the spatial resolution of CTP has increased considerably over the last decade and full brain coverage is possible with the newest generation of CT scanners, the usage of ionizing radiation needs to be considered as a significant health concern, especially in younger patients, given that a typical CTP series consists of 30–60 full 3D CT head scans. Furthermore, iodine-based contrast agents bear the risk of severe adverse allergic reactions (Bush & Swanson, 1991; see chapter 3). Both imaging sequences have additional drawbacks due to modality-specific artifacts during image acquisition. In CTP, metal artifacts can render the scans unusable for perfusion map quantification. DSC-PWI sequences can be affected by various artifacts such as contrast agent saturation, distortion, and eddy current effects, just to name a few. From a computational perspective, image sequences with a higher temporal resolution, and better signal-to-noise ratio than what can be achieved with DSC-PWI and especially CTP would be highly favorable. This would allow an improved calculation of the perfusion parameter maps with improved spatial and temporal accuracy. The determination of infarct core and the salvageable penumbra has gained additional importance in recent years. The accuracy and reliability of CT and MRI perfusion have recently been critically discussed (Huang et al., 2017). Defining the viable tissue through perfusion imaging is necessary to select optimal candidates for reperfusion therapy. However, the low temporal resolution of greater than 1 s per 3D image in standard CT and MRI perfusion imaging can significantly influence the quantification of salvageable tissue depending on the method and threshold parameters used, which might ultimately exclude patients of an optimal stroke treatment (Forkert et al., 2013). Multiband EPI acquisition provides a temporal resolution of less than 1 s, but multiband MRI scanners are expensive, and reconstruction of the parameter maps is time-consuming.

Due to the high temporal resolution coupled with the high-spatial-resolution and SNR, MPI allows 3D real-time imaging with high sensitivity at the submillimeter resolution without requiring ionizing radiation and toxic tracer material, making it a promising perfusion imaging technique. Some preclinical experiments have demonstrated the high potential of MPI for vascular imaging. In 2009, MPI captured the beating murine heart in real-time (J. Weizenecker et al., 2009). Recently, the perfusion of a human-sized organ was imaged with MPI ex vivo (Molwitz et al., 2019). However, the most significant progress in the last years was in the imaging of acute cerebrovascular diseases. The fast and accurate assessment of cerebral perfusion is fundamental for the successful treatment of stroke patients. So far, one preclinical stroke MPI study exists (Ludewig et al., 2017; see Figure 6). The murine stroke model used in this study mimics the occlusion of the middle cerebral artery (MCAO model). A silicone filament was inserted into the internal carotid artery and blocked the origin of the middle cerebral artery (MCA). A bolus of 20 μL SPIOs (LS008, c[Fe] = 46 mmol/L; see chapter 3) for the MPI, or 10 μL Gadolinium chelate for DSC-MRI, was injected via the tail vein. MPI scans (4D data with 21.5 ms temporal resolution, a selection field gradient strength of 2.5 T/m in one direction and 0.75 T/m in the remaining orthogonal directions, and a drive field [DF] amplitude of 14 mT) were acquired dynamically with 100% duty cycle while administering the contrast agent bolus. The MPI data had a physical resolution of about $3 \times 3 \times 1.5\ mm^3$.

This proof-of-concept study confirmed that MPI could detect small ischemic strokes of a few cubic millimeters with results comparable to a small-animal MRI scanner (see Figure 6a–c). The results could be reproduced in several animals ($n = 3$), and concentration–time curves were similar for each animal. The CBF dropped about 89.15% ± 1.33% (MPI) versus 91.52% ± 2.76% (MRI) in the ischemic hemispheres. These results agreed with the data of the laser Doppler during stroke induction, which showed a reduction of 87.32% ± 4.13% in the CBF. The CBV decrease in the ischemic hemispheres was 93.44% ± 5.01% (MPI) versus 90.14% ± 2.89% (MRI) compared with the contralateral hemispheres. The TTP was consistently prolonged by 85.85% ± 22.67% in MPI versus 89.26% ± 25.19% in MRI, and the MTT was extended by 22.89% ± 13.52% in MPI versus 36.72% ± 12.43% in MRI.

The main goal of the preclinical stroke study was to demonstrate that MPI can detect ischemic strokes similarly to MRI, which it did successfully. However, the drawback of the study is that it was impossible to calculate absolute perfusion parameters and prove the theoretical advantages of MPI due to the animal model and the low spatial resolution. A disadvantage of the MCAO model for imaging studies is the massive and constant drop of cerebral perfusion throughout the whole hemisphere with no definable penumbra by imaging (Ludewig et al., 2013). Additionally, the low spatial resolution made it difficult to obtain an accurate arterial input function. In theory, the excellent signal-to-noise ratio, and the spatial and temporal resolution of the MPI scanner, which exceeds current CTP and DSC-PWI imaging standards, could significantly improve the perfusion parameter map quantification that is required for clinical

decision-making. However, this would require that the MPI signal–time curves can be converted to absolute concentration–time curves, similar to the DSC-PWI signal–time curves. While it is possible to compute relative perfusion maps by normalization with the contralateral hemisphere after application of the deconvolution techniques used for the quantification of CTP and DSC-PWI perfusion maps (e.g., block circulant singular value decomposition), it is preferential to determine the absolute perfusion parameters in the brain as there are established absolute thresholds. By improving the spatial resolution to less than 1 mm with brain-specific MPI coils (Figure 6e; Graeser et al., 2019), calculating absolute perfusion parameters should become possible in animals. The first measurements in healthy animals were promising and showed increased cerebral blood flow in the cortex (Figure 6e) similar to ASL-MRI perfusion,

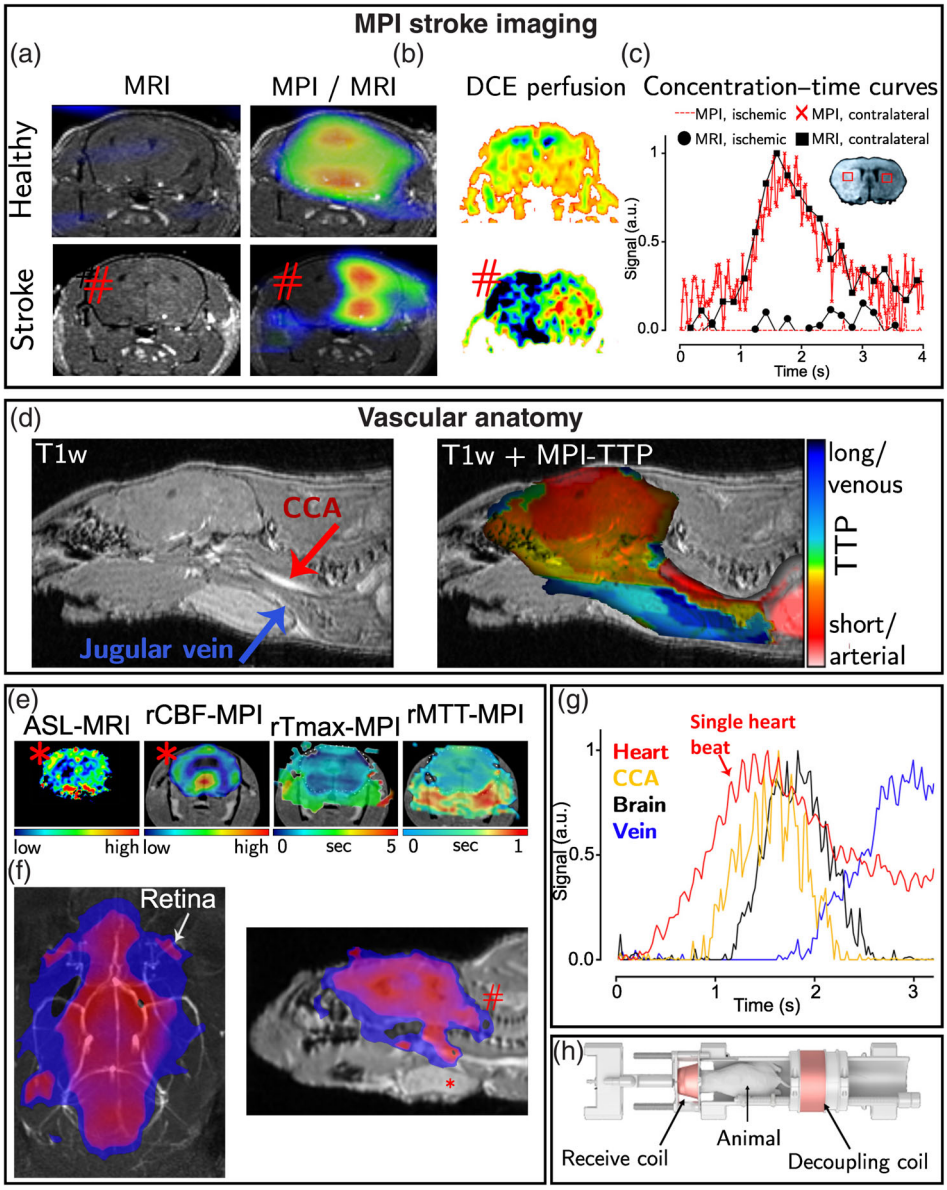

FIGURE 6 Imaging of cerebral perfusion with MPI. Cerebral perfusion was assessed with MPI (a,c) and compared with MRI (b,c). MPI clearly detected the ischemic stroke area (a, hash sign) similar to MRI (b). Concentration–time curves showed that MPI and MRI are comparable imaging techniques (c). Besides perfusion imaging, one bolus of contrast agent allows imaging of the vasculature and differentiation of arteries and veins (d). In the initial studies, spatial resolution was a limiting factor. Due to hardware improvement with a dedicated mouse head coil, the spatial resolution further improved while keeping the high temporal resolution. We can see the higher cortical perfusion with the head coil compared with the striatal perfusion, similar to ASL-perfusion (e). MPI also detects the retina's perfusion (f) and can differentiate between the anterior (f, asterisk) and posterior circulation (f, hash sign). The temporal resolution is fast enough to track the bolus from the heart to the common carotid artery (CCA), to the brain parenchyma into the veins (g). Reprinted with permission from Graeser et al. (2019) and Ludewig et al. (2017)

which was impossible in the pre-brain-coil era. Nevertheless, calibrated measurements with perfusion phantoms are mandatory before performing human studies.

In translating the data to humans, the spatial resolution of $3 \times 3 \times 1.5\ mm^3$ of the preclinical MPI scanner was sufficient to detect very small infarct volumes (e.g., 0.08 mL in the MCAO model versus 54 mL in typical supratentorial infarcts in patients). As human systems can be built with identical selection field strength (Jürgen Rahmer et al., 2018), the expected spatial resolution in a human-size torso image is in the same range. Additionally, the murine vessels occluded in the MCAO model range from 0.15 to 0.2 mm, which is still smaller than the M3 or M4 branches of the medial cerebral artery. Nevertheless, the sensitivity of MPI needs to be further evaluated in different stroke entities, such as lacunar or multiple small thromboembolic strokes.

The preclinical study also indicated the versatile capabilities of MPI and its possible advantages over DSC-PWI and CTP. With a single MPI tracer bolus, important information on perfusion, vascular anatomy, and heart rate was obtained within seconds (Figure 6d,g). In contrast, several different time-consuming sequences are necessary for an MRI to obtain similar data; for example, DSC-MRI for assessing the perfusion and time-of-flight or contrast-enhanced MR angiography for the imaging of the vasculature. Likewise, a CT scanner requires two shots of contrast agent for angiography and perfusion with a dose length product of 4300 mGy cm, which is four times higher than the annual radiation dose compared with the zero radiation of an MPI scanner. The additional acquisition and processing time for CT perfusion and CT angiography can be up to 15 min (Srinivasan et al., 2005). Assessing the MPI of stroke patients offers many other exciting possibilities. For example, it might be possible to determine the degree of stenosis by measuring blood flow velocities (Dietrich et al., 2021; Vaalma et al., 2017). MPI could also have great potential for detecting inflamed vulnerable plaques, allowing conclusions about the stroke's etiology, and further improving therapy (Tong et al., 2021).

4.2 | MPI of intracranial hemorrhage

Aside from ischemic strokes, other acute neurological conditions and stroke mimics require a rapid diagnosis. Since some of these conditions require different treatments, an essential prerequisite for the clinical application of MPI is the recognition and differentiation of these diseases. Intracranial hemorrhage is one of the most critical and frequent differential diagnoses that must be differentiated from ischemic stroke by MPI. Subtypes are intracerebral and subarachnoid hemorrhage (ICH and SAH), subsumed under hemorrhagic strokes, and epidural and subdural bleeds. With 4.1 million cases, ICH is common and accounts for approximately 20% of all strokes. The treatment of ischemic and hemorrhagic stroke differs significantly. More precisely, thrombolysis, which is used in ischemic stroke, is contraindicated in hemorrhage. Therefore, intracranial hemorrhage should be detected expeditiously by MPI without any additional imaging. A particular challenge in imaging hemorrhage is that MPI only detects tracers. Thus, hemorrhages that have not picked up tracer cannot be differentiated from ischemic stroke. Previous MPI studies circumvented this problem by injecting the tracer before induction of the bleeding in a model of traumatic brain injury (Orendorff et al., 2017). A recently published study on MPI of ICH took a more realistic approach (Szwargulski et al., 2020). In this model, bleeding was induced by collagenase injection (Figure 7).

As in daily clinical practice, the tracer was injected after the first bleeding occurred (30 min in this study). MPI detected the hemorrhage within 2.5 min on average (Figure 7a). This study showed that MPI can now clearly compete with conventional imaging techniques (e.g., T2-weighted MRI or non-contrast CT), with average stroke examination times of 11–13 min for CT and MRI (de Oliveira Manoel, 2020). In addition, the study also impressively demonstrated the use of multicontrast MPI. More precisely, it was possible to detect areas that were still fluid or already clotted within the hemorrhage. This information could help to understand whether bleeding is still active and whether surgical intervention is possible (Figure 7b).

Moreover, MPI enables simultaneous visualization of perfusion and hemorrhage. Thus, it is possible to determine the intracranial pressure noninvasively and whether healthy brain areas have sufficient perfusion (Figure 7c). The combined imaging of hemorrhage and perfusion is vital for patients with subarachnoid hemorrhage (SAH). In SAH, vasospasms of the cerebral arteries decrease cerebral perfusion, can cause a stroke, and require prompt treatment with vasodilators. MPI could detect these vasospasms early and lead to more rapid treatment. The detection of SAH with MPI has also been shown recently (Szwargulski et al., 2020). Studies on subdural and epidural hemorrhage using MPI do not yet exist. However, since the principles for MPI detection of these bleeding entities are similar to ICH, detection should be similarly successful. A disadvantage of these studies is that the bleedings were induced artificially. The prior

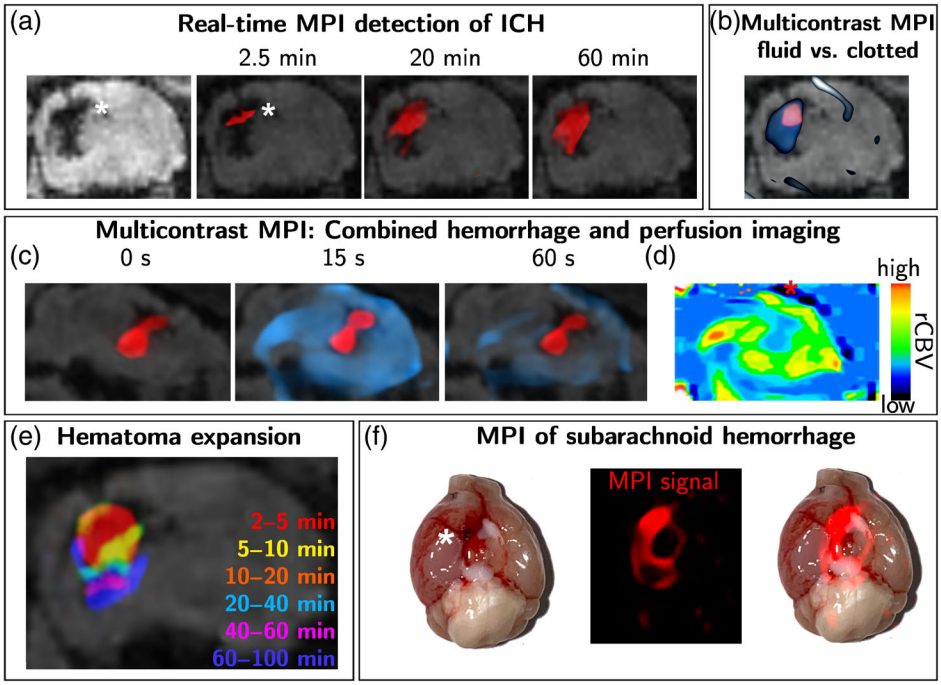

FIGURE 7 Imaging of intracerebral and subarachnoid hemorrhage with MPI. MPI quickly detects ICH within a few minutes (a). Continuous imaging allows monitoring of the hematoma expansion (a,e). Multicontrast MPI allows differentiation of fluid (b, blue) and clotted areas (b, red) within the hemorrhage. Multicontrast MPI can combine different tracers to monitor the hemorrhage (c, red) and assess the cerebral perfusion (c, blue). Calculation of the perfusion parameters maps shows perfusion deficits within the hemorrhage (d). Besides intracranial hemorrhage, MPI can detect subarachnoid bleeding (f; the asterisk shows the SAH on the left image; the image in the middle shows the MPI signal of the SAH in red; right image: Overlay). Reprinted with permission from Szwargulski et al. (2020)

knowledge of the localization of the hemorrhage facilitates detection. With spontaneous human hemorrhages, detection can become much more difficult, especially when the hemorrhage is no longer active. The hematoma would lead to reduced perfusion in this area, which could be detected with MPI. However, in the worst case, a hemorrhage cannot be distinguished from ischemia. Thus, more research is needed in this domain. Besides hemorrhages, it has been shown that MPI can also detect other stroke mimics, for example, brain tumors or metastasis, and epileptic seizures (Guduru et al., 2018; Meola et al., 2019).

5 | FORCE APPLICATION WITH MPI TO IMPROVE STROKE THERAPY

Originally, MPI was proposed as a diagnostic imaging technique (Knopp et al., 2017). The unique gradient electromagnet design inherently adds the possibility of applying magnetic forces and torques. Both can be generated with an MPI scanner in a flexible and spatially selective manner, which offers a wide range of medical applications. For instance, it is possible to navigate nanoparticles or ferromagnetic devices to the desired positions in a patient's body in a contactless fashion only by controlling the applied magnetic fields.

When combining an MPI scanner's imaging and force capabilities, direct spatial feedback of the applied force and, therefore, direct position control can be obtained.

There are two ways to change the state of motion of a ferromagnetic object via a magnetic field. It is possible to apply a torque $\vec{T} = \vec{m} \times \vec{B}$ or a force $\vec{F} = \nabla\left(\vec{m} \cdot \vec{B}\right)$ to the object's dipole moment $\vec{m}$, where $\vec{B}$ is the magnetic flux density. The orthogonal component of $\vec{m}$ in respect to $\vec{B}$ results in the torque $\vec{T}$ forcing it to align with the magnetic field. The parallel component of $\vec{m}$ in respect to $\vec{B}$ results in the force $\vec{F}$ driving the magnetic moment toward regions of higher field strength. In homogeneous magnetic fields, the force $\vec{F}$ vanishes as the gradient in the equation above is zero. If the selection field generator is designed as a flexible gradient and focus field generator, the generation of arbitrarily shifted gradient fields is possible. This setup makes it possible to apply various dedicated forces and torques by precise control of the applied magnetic fields.

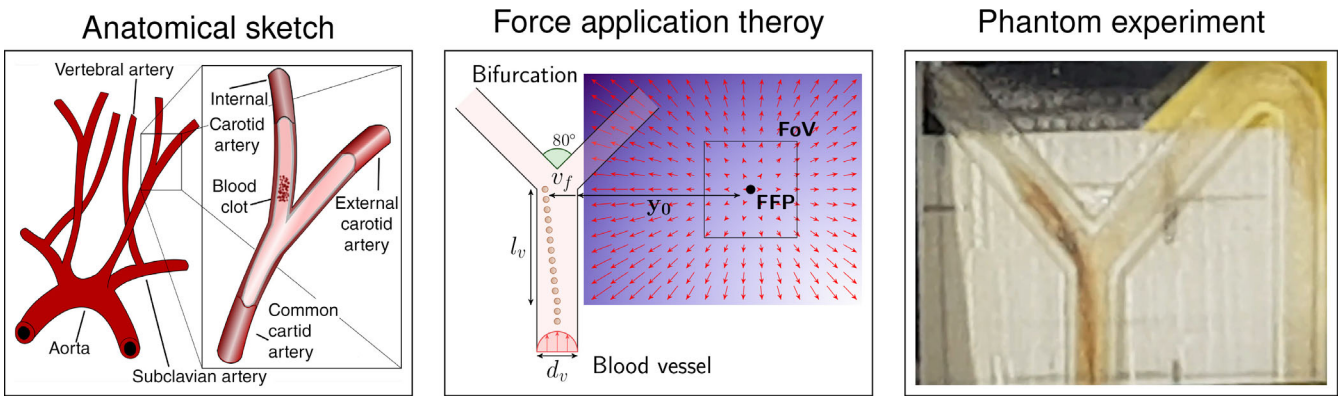

FIGURE 8 Flow experiments for targeted drug delivery with MPI. Left: A stenosis caused by a blood clot in the internal carotid artery. Centre: Schematic drawing of a flow experiment in a branched blood vessel. By moving the FFP away from the vessel, a high force is exerted on the nanoparticles. Using this force, the particles can be directed into one of the two branches. Right: Photo taken during the experiment. It is visible that the brown-colored particles accumulate on the left side of the vessel due to the magnetic field, although there is no flow in the left arm of the vessel because of a 100% stenosis. Reprinted with permission from Griese et al. (2020)

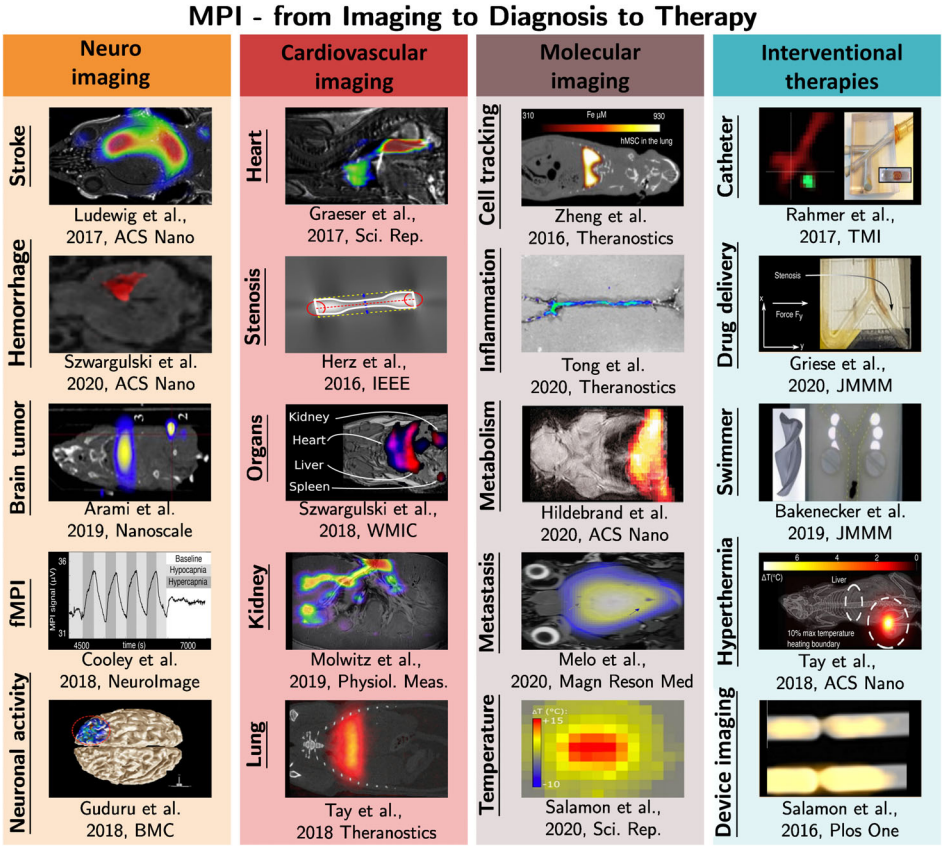

FIGURE 9 MPI—from imaging to diagnosis to therapy. The figure provides an overview of preclinical MPI applications

There are two main approaches for moving nanoparticles and microdevices with an MPI scanner based on these possibilities: The first approach essentially uses the field gradient to exert a directional force. The second approach uses rotating magnetic fields to generate torque on small devices like microswimmers, translating the torque into a directional movement.

Utilizing the gradient-based method, a phantom consisting of six soft magnetic spheres allowed guiding of the magnetic device into different target areas, whereas the position was adjusted using real-time MPI images and a control loop

(Nothnagel et al., 2016). Based on this work, Rahmer et al. demonstrated the navigation of a magnetically coated catheter through a vessel phantom (Rahmer, Stehning, & Gleich, 2017; Rahmer, Wirtz, et al., 2017). The tip of the catheter was equipped with a magnetic sphere, which steered the catheter in different directions. Simultaneously, the catheter's coating could be imaged, giving direct feedback on its position. By exploiting multicontrast MPI, it was also possible to distinguish between the catheter and the particles inside the phantom in the MPI images (J. Haegele, Vaalma, et al., 2016; Muslu et al., 2018).

The force for soft magnetic materials below their saturation increases linearly with the field strength because $\vec{m}$ is changing with the applied field. This effect makes it possible to modulate the force on the sphere by changing the distance between the FFP and the catheter tip. MPI could enable real-time tomographic tracking and magnetic guidance of catheters to assist physicians during interventions. In acute ischemic stroke treatment, mechanical thrombectomy of blood clots is the current standard of practice. Unfortunately, this treatment is only available at large clinical centers. Remote control of catheters using MPI could thus enable thrombectomy in sparsely populated regions.

In addition to the manipulation of macroscopic instruments, it has also been shown that force MPI can be used for targeted drug delivery. Therapeutic substances can be attached to nanoparticles and be guided to regions where the drugs can act locally (Griese et al., 2020). This magnetic drug targeting is a promising approach to deliver therapeutic agents more efficiently so that SPIOs coupled to drugs can be directed to a target volume, for example, the blood clot in an occluded vessel, by external magnetic fields.

A promising step was the introduction of two-dimensional real-time monitoring for a magnetic nanoparticle guidance system (Le et al., 2017). Later it was shown that the magnetic force could be adjusted by controlling the FFP with the help of a joystick or mouse in real-time (Bui et al., 2020). There were further investigations on suitable tracers for MPI force applications and simultaneous imaging (Griese et al., 2020). In a phantom of the bifurcation of the common carotid artery, this study showed that particles could be navigated into the branch of an occluded vessel against the blood flow (see Figure 8). Disturbed flow conditions due to vessel occlusion prevent rt-PA from reaching the blood clot in sufficient concentrations. Within this context, targeted thrombolysis of clots in acute ischemic stroke patients might be of high interest. In vitro experiments demonstrated that thrombolysis time could be reduced by almost half by concentrating rt-PA-SPIOs on the blood clot (Yang et al., 2012), which could dramatically improve stroke outcomes. At the same time, targeted thrombolysis could also enable to lower the dosage of thrombolysis drugs leading to reduced local and systemic side effects, such as hemorrhage. Targeted drug delivery with MPI is still a young research field within the MPI community, and a lot of effort must be made to eventually achieve clinical translation in the future.

However, these studies highlight that MPI is not just an alternative imaging technique to MRI or CT but has much more to offer. MPI covers the entire spectrum of imaging requirements for the diagnosis of cerebrovascular diseases while also simultaneously enabling new therapeutic approaches.

6 | CONCLUSION

MPI is a groundbreaking technology still in its very early stages. However, there have been significant technical improvements and progress in preclinical MPI applications in the last few years (see Figure 9). Early MPI research prioritized cancer research, but neurological and neurovascular applications, especially stroke imaging, are currently coming into focus. It is important to emphasize that MPI covers the entire spectrum of imaging requirements for the diagnosis of cerebrovascular diseases and also provides new therapeutic options through targeted delivery of drugs or catheters. These applications are still experimental on various levels, but they demonstrate a wide range of new therapeutic opportunities to treat neurological diseases. But how can we envision the future clinical deployment of MPI? It is unlikely that MPI will replace standard MRI or CT imaging, as they are excellent in their applications. But we see a niche for MPI in the clinical routine: A significant advantage in this context is that MPI scanners can be built as small mobile units for continuous bedside use. To date, a fast, reliable method allowing continuous bedside monitoring of whole-brain perfusion does not exist. Patient surveillance has typically been noninvasive through clinical examination, but this cannot be done continuously. MPI could close this gap in health care and enable noninvasive, permanent monitoring of patients and faster interventions in case of deterioration. Given the potential for miniaturization, MPI might become a cheap alternative for bedside perfusion imaging in the emergency room and stroke and intensive care units. Much development is necessary to improve imager design, tracer

design, and imaging protocols. With these improvements and the upcoming development of human-sized scanners, MPI can become a widely adopted clinical tool for neuroimaging.

ACKNOWLEDGMENTS

This work was supported by the "Forschungszentrums Medizintechnik Hamburg" (FMTHH) by the Hertie-Stiftung (Hertie Academy of Clinical Neuroscience), the German Research Foundation (DFG; grant numbers: GR 5287/2–1, KN 1108/7–1, DFG FOR 2879 [project LU 1924/1–1 and MA 4375/6–1]), and the "Hermann und Lily Schilling Stiftung". This work was also supported by the BMBF under the frame of EuroNanoMed III (grant number: 13XP5060B, "Magnetize").

CONFLICT OF INTEREST

The authors have declared no conflicts of interest for this article.

AUTHOR CONTRIBUTIONS

Peter Ludewig: Conceptualization (lead); funding acquisition (lead); investigation (lead); methodology (lead); project administration (lead); resources (lead); software (supporting); supervision (equal); validation (lead); visualization (lead); writing – original draft (lead); writing – review and editing (lead). **Matthias Graeser:** Conceptualization (lead); investigation (lead); methodology (lead); project administration (lead); resources (lead); software (lead); supervision (lead); validation (lead); visualization (lead); writing – original draft (lead); writing – review and editing (lead). **Nils Daniel Forkert:** Conceptualization (lead); software (lead); supervision (lead); validation (lead); visualization (lead); writing – original draft (lead); writing – review and editing (lead). **Florian Thieben:** Writing – original draft (supporting). **Fynn Förger:** Writing – original draft (supporting). **Javier Rández-Garbayo:** Writing – original draft (supporting). **Johanna Rieckhoff:** Writing – review and editing (supporting). **Katrin Lessmann:** Writing – review and editing (supporting). **Patryk Szwargulski:** Writing – original draft (supporting). **Tim Magnus:** Writing – original draft (lead); writing – review and editing (lead). **Tobias Knopp:** Conceptualization (lead); data curation (lead); formal analysis (lead); funding acquisition (lead); investigation (lead); methodology (lead); project administration (lead); supervision (lead); writing – original draft (lead); writing – review and editing (lead).

DATA AVAILABILITY STATEMENT

Data sharing is not applicable to this article as no new data were created or analyzed in this study.

ORCID

Peter Ludewig https://orcid.org/0000-0001-9025-6402
Matthias Graeser https://orcid.org/0000-0003-1472-5988
Nils D. Forkert https://orcid.org/0000-0003-2556-3224
Florian Thieben https://orcid.org/0000-0002-2890-5288
Johanna Rieckhoff https://orcid.org/0000-0002-6336-8481

FURTHER READING

Bakenecker, A. C., von Gladiss, A., Friedrich, T., Heinen, U., Lehr, H., Lüdtke-Buzug, K., & Buzug, T. M. (2019). Actuation and visualization of a magnetically coated swimmer with magnetic particle imaging. *Journal of Magnetism and Magnetic Materials*, *473*, 495–500. https://doi.org/10.1016/j.jmmm.2018.10.056

Bente, K., Codutti, A., Bachmann, F., & Faivre, D. (2018). Biohybrid and bioinspired magnetic microswimmers. *Small*, *14*(29), 1704374. https://doi.org/10.1002/smll.201704374

Kaul, M. G., Salamon, J., Knopp, T., Ittrich, H., Adam, G., Weller, H., & Jung, C. (2018). Magnetic particle imaging for in vivo blood flow velocity measurements in mice. *Physics in Medicine & Biology*, *63*(6), 064001. https://doi.org/10.1088/1361-6560/aab136

Kjølby, B. F., Østergaard, L., & Kiselev, V. G. (2006). Theoretical model of intravascular paramagnetic tracers effect on tissue relaxation. *Magnetic Resonance in Medicine*, *56*(1), 187–197. https://doi.org/10.1002/mrm.20920

Schmale, I., Gleich, B., Schmidt, J., Rahmer, J., Bontus, C., Eckart, R., David, B., Heinrich, M., Mende, O., Woywode, O., Jokram, J., & Borgert, J. (2013). Human PNS and SAR study in the frequency range from 24 to 162 kHz. International workshop on magnetic particle imaging, IWMPI 2013.

Shasha, C., Teeman, E., Krishnan, K. M, Szwargulski, P., Knopp, T., & Möddel, M. (2019). Discriminating nanoparticle core size using multi-contrast MPI. *Physics in Medicine & Biology*, *64*(7), 074001. https://doi.org/10.1088/1361-6560/ab0fc9

REFERENCES

Adkinson, N. F., Strauss, W. E., Macdougall, I. C., Bernard, K. E., Auerbach, M., Kaper, R. F., Chertow, G. M., & Krop, J. S. (2018). Comparative safety of intravenous ferumoxytol versus ferric carboxymaltose in iron deficiency anemia: A randomized trial. *American Journal of Hematology*, *93*(5), 683–690. https://doi.org/10.1002/ajh.25060

Antonelli, A., Sfara, C., Weber, O., Pison, U., Manuali, E., Salamida, S., & Magnani, M. (2016). Characterization of ferucarbotran-loaded RBCs as long circulating magnetic contrast agents. *Nanomedicine*. https://doi.org/10.2217/nnm-2016-0216

Antonelli, A., Szwargulski, P., Scarpa, E.-S., Thieben, F., Cordula, G., Ambrosi, G., Guidi, L., Ludewig, P., Knopp, T., & Magnani, M. (2020). Development of long circulating magnetic particle imaging tracers: Use of novel magnetic nanoparticles and entrapment into human erythrocytes. *Nanomedicine*, *15*(8), 739–753. https://doi.org/10.2217/nnm-2019-0449

Arsalani, S., Löwa, N., Kosch, O., Radon, P., Baffa, O., & Wiekhorst, F. (2021). Magnetic separation of iron oxide nanoparticles to improve their application for magnetic particle imaging. *Physics in Medicine & Biology*, *66*(1), 015002. https://doi.org/10.1088/1361-6560/abcd19

Baird, A. E., Benfield, A., Schlaug, G., Siewert, B., Lövblad, K. O., Edelman, R. R., & Warach, S. (1997). Enlargement of human cerebral ischemic lesion volumes measured by diffusion-weighted magnetic resonance imaging. *Annals of Neurology*, *41*(5), 581–589. https://doi.org/10.1002/ana.410410506

Behzadi, A. H., Zhao, Y., Farooq, Z., & Prince, M. R. (2018). Immediate allergic reactions to gadolinium-based contrast agents: A systematic review and meta-analysis. *Radiology*, *286*(2), 471–482. https://doi.org/10.1148/radiol.2017162740

Bender, P., Fock, J., Frandsen, C., Hansen, M. F., Balceris, C., Ludwig, F., Posth, O., Wetterskog, E., Bogart, L. K., Southern, P., Szczerba, W., Zeng, L., Witte, K., Grüttner, C., Westphal, F., Honecker, D., González-Alonso, D., Fernández Barquín, L., & Johansson, C. (2018). Relating magnetic properties and high hyperthermia performance of iron oxide Nanoflowers. *The Journal of Physical Chemistry C*, *122*(5), 3068–3077. https://doi.org/10.1021/acs.jpcc.7b11255

Biederer, S., Knopp, T., Sattel, T. F., Lüdtke-Buzug, K., Gleich, B., Weizenecker, J., Borgert, J., & Buzug, T. M. (2009). Magnetization response spectroscopy of superparamagnetic nanoparticles for magnetic particle imaging. *Journal of Physics D: Applied Physics*, *42*(20), 205007. https://doi.org/10.1088/0022-3727/42/20/205007

Bontus, C., Gleich, B., David, B., Mende, O., & Borgert, J. (2015). Concept of a generator for the selection and focus field of a clinical MPI scanner. *IEEE Transactions on Magnetics*, *51*(2), 1–4. https://doi.org/10.1109/TMAG.2014.2326003

Bui, M. P., Le, T.-A., & Yoon, J. (2021). A magnetic particle imaging-based navigation platform for magnetic nanoparticles using interactive manipulation of a virtual field free point to ensure targeted drug delivery. *IEEE Transactions on Industrial Electronics*, *68*(12), 12493–12503. https://doi.org/10.1109/tie.2020.3039219

Bulte, J. W.M. (2019). Superparamagnetic iron oxides as MPI tracers: A primer and review of early applications. *Advanced Drug Delivery Reviews*, *138*, 293–301. https://doi.org/10.1016/j.addr.2018.12.007

Bush, W. H., & Swanson, D. P. (1991). Acute reactions to intravascular contrast media: Types, risk factors, recognition, and specific treatment. *American Journal of Roentgenology*, *157*(6), 1153–1161 https://doi.org/10.2214/ajr.157.6.1950858

Campbell, B. C. V., Christensen, S., Levi, C. R., Desmond, P. M., Donnan, G. A., Davis, S. M., & Parsons, M. W. (2011). Cerebral blood flow Is the optimal CT perfusion parameter for assessing infarct core. *Stroke*, *42*, 3435–40. https://doi.org/10.1161/STROKEAHA.111.618355

Chandrasekharan, P., Tay, Z. W., Hensley, D., Zhou, X. Y., Fung, B. K., Colson, C., Lu, Y., Fellows, B. D., Huynh, Q., Saayujya, C., Yu, E., Orendorff, R., Zheng, B., Goodwill, P., Rinaldi, C., & Conolly, S. (2020). Using magnetic particle imaging systems to localize and guide magnetic hyperthermia treatment: Tracers, hardware, and future medical applications. *Theranostics*, *10*(7), 2965–2981. https://doi.org/10.7150/thno.40858

Cochran, S. T. (2005). Anaphylactoid reactions to radiocontrast media. *Current Allergy and Asthma Reports*, *5*(1), 28–31 https://doi.org/10.1007/s11882-005-0051-7

Cooley, C. Z., Mandeville, J. B., Mason, E. E., Mandeville, E.T., & Wald, L. L. (2018). Rodent Cerebral Blood Volume (CBV) changes during hypercapnia observed using Magnetic Particle Imaging (MPI) detection. *NeuroImage*, *178*, 713–720. https://doi.org/10.1016/j.neuroimage.2018.05.004

Dadfar, S. M., Camozzi, D., Darguzyte, M., Roemhild, K., Varvarà, P., Metselaar, J., Banala, S., Straub, M., Güvener, N., Engelmann, U., Slabu, I., Buhl, M., van Leusen, J., Kögerler, P., Hermanns-Sachweh, B., Schulz, V., Kiessling, F., & Lammers, T. (2020). Size-isolation of superparamagnetic iron oxide nanoparticles improves MRI, MPI and hyperthermia performance. *Journal of Nanobiotechnology*, *18*(1), 22. https://doi.org/10.1186/s12951-020-0580-1

de Oliveira Manoel, A. L. (2020). Surgery for spontaneous intracerebral hemorrhage. *Critical Care (London, England)*, *24*(1), 45. https://doi.org/10.1186/s13054-020-2749-2

Dietrich, P., Vogel, P., Kampf, T., Rückert, M. A., Behr, V. C., Bley, T. A., & Herz, S. (2021). Near real-time magnetic particle imaging for visual assessment of vascular stenosis in a phantom model. *Physica Medica*, *81*, 210–214. https://doi.org/10.1016/j.ejmp.2020.12.020

Draack, S., Schilling, M., & Viereck, T. (2021). Magnetic particle imaging of particle dynamics in complex matrix systems. *Physical Sciences Reviews*. https://doi.org/10.1515/psr-2019-0123

Du, Y., Liu, X., Liang, Q., Liang, X.-J., & Tian, J. (2019). Optimization and Design of Magnetic Ferrite Nanoparticles with Uniform Tumor Distribution for Highly Sensitive MRI/MPI Performance and Improved Magnetic Hyperthermia Therapy. *Nano Letters*, *19*(6), 3618–3626. https://doi.org/10.1021/acs.nanolett.9b00630

Erathodiyil, N., & Ying, J. Y. (2011). Functionalization of inorganic nanoparticles for bioimaging applications. *Accounts of Chemical Research*, *44*(10), 925–935. https://doi.org/10.1021/ar2000327

Ferguson, R. M., Khandhar, A. P., Arami, H., Hua, L., Hovorka, O., & Krishnan, K. M. (2013). Tailoring the magnetic and pharmacokinetic properties of iron oxide magnetic particle imaging tracers. *Biomedical Engineering*, *58*(6), 493–507. https://doi.org/10.1515/bmt-2012-0058

Forkert, N. D., Cheng, B., Kemmling, A., Thomalla, G., & Fiehler, J. (2014). ANTONIA perfusion and stroke. A software tool for the multi-purpose analysis of MR perfusion-weighted datasets and quantitative ischemic stroke assessment. *Methods of Information in Medicine*, *53*(6), 469–481. https://doi.org/10.3414/ME14-01-0007

Forkert, N. D., Kaesemann, P., Treszl, A., Siemonsen, S., Cheng, B., Handels, H., Fiehler, J., & Thomalla, G. (2013). Comparison of 10 TTP and Tmax Estimation Techniques for MR Perfusion-Diffusion Mismatch Quantification in Acute Stroke. *American Journal of Neuroradiology*, *34*(9), 1697–1703. https://doi.org/10.3174/ajnr.a3460

Franke, J., Baxan, N., Lehr, H., Heinen, U., Reinartz, S., Schnorr, J., Heidenreich, M., Kiessling, F., & Schulz, V. (2020). Hybrid MPI-MRI System for Dual-Modal In Situ Cardiovascular Assessments of Real-Time 3D Blood Flow Quantification—A Pre-Clinical In Vivo Feasibility Investigation. *IEEE Transactions on Medical Imaging*, *39*(12), 4335–4345. https://doi.org/10.1109/tmi.2020.3017160

Franke, J., Heinen, U., Lehr, H., Weber, A., Jaspard, F., Ruhm, W., Heidenreich, M., & Schulz, V. (2016). System characterization of a highly integrated preclinical hybrid MPI-MRI scanner. *IEEE Transactions on Medical Imaging*, *35*(9), 1993–2004. https://doi.org/10.1109/TMI.2016.2542041

Gdaniec, N., Boberg, M., Moddel, M., Szwargulski, P., & Knopp, T. (2020). Suppression of motion artifacts caused by temporally recurring tracer distributions in multi-patch magnetic particle imaging. *IEEE Transactions on Medical Imaging*, *39*(11), 3548–3558. https://doi.org/10.1109/TMI.2020.2998910

Gleich, B., Weizenecker, J., Timminger, H., Bontus, C., Schmale, I., Rahmer, J., Schmidt, J., Kanzenbach, J., & Borgert, J. (2010). Fast MPI demonstrator with enlarged field of view. *Proceedings of the International Society for Magnetic Resonance in Medicine (ISMRM)*, *18*, 218.

Gleich, B., & Weizenecker, J. (2005). Tomographic imaging using the nonlinear response of magnetic particles. *Nature*, *435*(7046), 1214–1217. https://doi.org/10.1038/nature03808

Goodwill, P. W., Konkle, J. J., Bo Zheng, Saritas, E. U., & Conolly, S. T. (2012). Projection X-Space Magnetic Particle Imaging. *IEEE Transactions on Medical Imaging*, *31*(5), 1076–1085. https://doi.org/10.1109/tmi.2012.2185247

Graeser, M., Bente, K., & Buzug, T. M. (2015). Dynamic single-domain particle model for magnetite particles with combined crystalline and shape anisotropy. *Journal of Physics D: Applied Physics*, *48*(27), 275001. https://doi.org/10.1088/0022-3727/48/27/275001

Graeser, M., Bente, K, Neumann, A., Buzug, T. M. (2016). Trajectory dependent particle response for anisotropic mono domain particles in magnetic particle imaging. *Journal of Physics D: Applied Physics*, *49*(4), 045007. https://doi.org/10.1088/0022-3727/49/4/045007

Graeser, M., Thieben, F., Szwargulski, P., Werner, F., Gdaniec, N., Boberg, M., Griese, F., Möddel, M., Ludewig, P., van de Ven, D., Weber, O. M., Woywode, O., Gleich, B., & Knopp, T. (2019). Human-sized magnetic particle imaging for brain applications. *Nature Communications*, *10*(1), https://doi.org/10.1038/s41467-019-09704-x

Graeser, M., Knopp, T., Szwargulski, P., Friedrich, T., von Gladiss, A., Kaul, M., Krishnan, K. M, Ittrich, H., Adam, G., & Buzug, T. M. (2017). Towards picogram detection of superparamagnetic iron-oxide particles using a gradiometric receive coil. *Scientific Reports*, *7*(1), https://doi.org/10.1038/s41598-017-06992-5

Graeser, M., Ludewig, P., Szwargulski, P., Foerger, F., Liebing, T., Forkert, N. D., Thieben, F., Magnus, T., & Knopp, T. (2020). Design of a head coil for high resolution mouse brain perfusion imaging using magnetic particle imaging. *Physics in Medicine & Biology*, *65*(23), 235007. https://doi.org/10.1088/1361-6560/abc09e

Griese, F., Knopp, T., Gruettner, C., Thieben, F., Müller, K., Loges, S., Ludewig, P., & Gdaniec, N. (2020). Simultaneous magnetic particle imaging and navigation of large superparamagnetic nanoparticles in bifurcation flow experiments. *Journal of Magnetism and Magnetic Materials*, *498*, 166206. https://doi.org/10.1016/j.jmmm.2019.166206

Griese, F., Latus, S., Schlüter, M., Graeser, M., Lutz, M., Schlaefer, A., Knopp, T. (2020). In-Vitro MPI-guided IVOCT catheter tracking in real time for motion artifact compensation. *PLOS ONE*, *15*(3), e0230821. https://doi.org/10.1371/journal.pone.0230821

Grüttner, M., Knopp, T., Franke, J., Heidenreich, M., Rahmer, J., Halkola, A., Kaethner, C., Borgert, J., & Buzug, T. M. (2013). On the formulation of the image reconstruction problem in magnetic particle imaging. *Biomedizinische Technik/Biomedical Engineering*, *58*(6), https://doi.org/10.1515/bmt-2012-0063

Guduru, R., Liang, P., Yousef, M., Horstmyer, J., & Khizroev, S. (2018). Mapping the brain's electric fields with magnetoelectric nanoparticles. *Bioelectronic Medicine*, *4*, 10. https://doi.org/10.1186/s42234-018-0012-9

Guo, B. J., Yang, Z. L., & Zhang, L. J. (2018). Gadolinium deposition in brain: Current scientific evidence and future perspectives. *Frontiers in Molecular Neuroscience*, *11*, 335. https://doi.org/10.3389/fnmol.2018.00335

Guzy, J., Chakravarty, S., Buchanan, F. J., Chen, H., Gaudet, J.M., Hix, J.M. L., Mallett, C. L., & Shapiro, E.M. (2020). Complex relationship between iron oxide nanoparticle degradation and the signal intensity in magnetic particle imaging. *ACS Applied Nano Materials*, *3*(5), 3991–3999. https://doi.org/10.1021/acsanm.0c00779

Haegele, J., Panagiotopoulos, N., Cremers, S., Rahmer, J., Franke, J., Duschka, R. L., Vaalma, S., Heidenreich, M., Borgert, J., Borm, P., Barkhausen, J., & Vogt, F. M. (2016). Magnetic particle imaging: A resovist based marking technology for guide wires and catheters for vascular interventions. *IEEE Transactions on Medical Imaging*, *35*(10), 2312–2318. https://doi.org/10.1109/TMI.2016.2559538

Haegele, J., Vaalma, S., Panagiotopoulos, N., Barkhausen, J., Vogt, F. M., Borgert, J., & Rahmer, J. (2016). Multi-color magnetic particle imaging for cardiovascular interventions. *Physics in Medicine and Biology*, *61*(16), N415–N426. https://doi.org/10.1088/0031-9155/61/16/N415

Hamm, B., Staks, T., Taupitz, M., Maibauer, R., Speidel, A., Huppertz, A., Frenzel, T., Lawaczeck, R., Wolf, K. J., & Lange, L. (1994). Contrast-enhanced MR imaging of liver and spleen: First experience in humans with a new superparamagnetic iron oxide. *Journal of Magnetic Resonance Imaging*, *4*(5), 659–668. https://doi.org/10.1002/jmri.1880040508

Hetzel, D., Strauss, W., Bernard, K., Li, Z., Urboniene, A., & Allen, L. F. (2014). A Phase III, randomized, open-label trial of ferumoxytol compared with iron sucrose for the treatment of iron deficiency anemia in patients with a history of unsatisfactory oral iron therapy. *American Journal of Hematology*, *89*(6), 646–650 https://doi.org/10.1002/ajh.23712

Hildebrand, S., Löwa, N., Paysen, H., Fratila, R. M., Reverte-Salisa, L., Trakoolwilaiwan, T., Niu, Z., Kasparis, G., Preuss, S. F., Kosch, Ol., M. de la Fuente, J., Thanh, N. T. K., Wiekhorst, F., & Pfeifer, A. (2021). Quantification of lipoprotein uptake in vivo using magnetic particle imaging and spectroscopy. *ACS Nano*, *15*(1), 434–446. https://doi.org/10.1021/acsnano.0c03229

Hola, K., Markova, Z., Zoppellaro, G., Tucek, J., & Zboril, R. (2015). Tailored functionalization of iron oxide nanoparticles for MRI, drug delivery, magnetic separation and immobilization of biosubstances. *Biotechnology Advances*, *33*(6), 1162–1176. https://doi.org/10.1016/j.biotechadv.2015.02.003

Huang, X., Kalladka, D., Cheripelli, B. K., Moreton, F. C., & Muir, K. W. (2017). The impact of CT perfusion threshold on predicted viable and nonviable tissue volumes in acute ischemic stroke. *Journal of Neuroimaging*, *27*(6), 602–606. https://doi.org/10.1111/jon.12442

Iv, M., Ng, N. N., Nair, S., Zhang, Y., Lavezo, J., Cheshier, S. H., Holdsworth, S. J., Moseley, M. E., Rosenberg, J., Grant, G. A., & Yeom, K. W. (2020). Brain iron assessment after ferumoxytol-enhanced MRI in children and young adults with arteriovenous malformations: A case-control study. *Radiology*, *297*(2), 438–446 https://doi.org/10.1148/radiol.2020200378

Kanda, T., Ishii, K., Kawaguchi, H., Kitajima, K., & Takenaka, D. (2014). High signal intensity in the dentate nucleus and globus pallidus on unenhanced T1-weighted MR images: Relationship with increasing cumulative dose of a gadolinium-based contrast material. *Radiology*, *270*(3), 834–841. https://doi.org/10.1148/radiol.13131669

Karpavičius, A., Coene, A., Bender, P., & Leliaert, J. (2021). Advanced analysis of magnetic nanoflower measurements to leverage their use in biomedicine. *Nanoscale Advances*, *3*, 1633–1645. https://doi.org/10.1039/D0NA00966K

Kaul, M. G., Mummert, T., Jung, C., Salamon, J., Khandhar, A.P, Ferguson, R M., Kemp, S. J, Ittrich, H., Krishnan, K. M, Adam, G., & Knopp, T. (2017). In vitro and in vivo comparison of a tailored magnetic particle imaging blood pool tracer with Resovist. *Physics in Medicine and Biology*, *62*(9), 3454–3469. https://doi.org/10.1088/1361-6560/aa5780

Keselman, P., Yu, E. Y, Zhou, X. Y., Goodwill, P. W., Chandrasekharan, P., Ferguson, R M., Khandhar, A. P, Kemp, S. J, Krishnan, K. M, Zheng, B., & Conolly, S. M (2017). Tracking short-term biodistribution and long-term clearance of SPIO tracers in magnetic particle imaging. *Physics in Medicine and Biology*, *62*(9), 3440–3453. https://doi.org/10.1088/1361-6560/aa5f48

Khandhar, A. P., Keselman, P., Kemp, S. J., Ferguson, R. M., Goodwill, P. W., Conolly, S. M., & Krishnan, K. M. (2017). Evaluation of PEG-coated iron oxide nanoparticles as blood pool tracers for preclinical magnetic particle imaging. *Nanoscale*, *9*(3), 1299–1306. https://doi.org/10.1039/c6nr08468k

Khandhar, A. P., Ferguson, R. M., Arami, H., Kemp, S. J., & Krishnan, K. M. (2015). Tuning surface coatings of optimized magnetite nanoparticle tracers for *in vivo* magnetic particle imaging. *IEEE Transactions on Magnetics*, *51*(2), 1–4. https://doi.org/10.1109/tmag.2014.2321096

Knopp, T., Biederer, S., Sattel, T., Weizenecker, J., Gleich, B., Borgert, J., & Buzug, T. M. (2009). Trajectory analysis for magnetic particle imaging. *Physics in Medicine and Biology*, *54*(2), 385–397. https://doi.org/10.1088/0031-9155/54/2/014

Knopp, T., Gdaniec, N., & Möddel, M. (2017). Magnetic particle imaging: From proof of principle to preclinical applications. *Physics in Medicine & Biology*, *62*(14), R124–R178. https://doi.org/10.1088/1361-6560/aa6c99

Knopp, T., Rahmer, J., Sattel, T. F., Biederer, S., Weizenecker, J., Gleich, B., Borgert, J., & Buzug, T. M. (2010). Weighted iterative reconstruction for magnetic particle imaging. *Physics in Medicine and Biology*, *55*(6), 1577–1589. https://doi.org/10.1088/0031-9155/55/6/003

Knopp, T., Biederer, S., Sattel, T. F., Erbe, M., & Buzug, T. M. (2011). Prediction of the spatial resolution of magnetic particle imaging using the modulation transfer function of the imaging process. *IEEE Transactions on Medical Imaging*, *30*(6), 1284–1292. https://doi.org/10.1109/TMI.2011.2113188

Kratz, H., Taupitz, M., Ariza de Schellenberger, A., Kosch, O., Eberbeck, D., Wagner, S., Trahms, L., Hamm, B., & Schnorr, J. (2018). Novel magnetic multicore nanoparticles designed for MPI and other biomedical applications: From synthesis to first in vivo studies. *PLoS One*, *13*(1), e0190214. https://doi.org/10.1371/journal.pone.0190214

Latus, S., Griese, F., Schlüter, M., Otte, C., Möddel, M., Graeser, M., Saathoff, T., Knopp, T., & Schlaefer, A. (2019). Bimodal intravascular volumetric imaging combining OCT and MPI. *Medical Physics*, *46*(3), 1371–1383. https://doi.org/10.1002/mp.13388

Lawaczeck, R., Bauer, H., Frenzel, T., Hasegawa, M., Ito, Y., Kito, K., Miwa, N., Tsutsui, H., Vogler, H., & Weinmann, H.-J. (1997). Magnetic iron oxide particles coated with carboxydextran for parenteral administration and liver contrasting. *Acta Radiologica*, *38*(4), 584–597. https://doi.org/10.1080/02841859709174391

Le, T.-A., Zhang, X., Hoshiar, A. K., & Yoon, J. (2017). Real-time two-dimensional magnetic particle imaging for electromagnetic navigation in targeted drug delivery. *Sensors*, *17*(9), 2050. https://doi.org/10.3390/s17092050

Liu, Z., Kiessling, F., & Gätjens, J. (2010). Advanced nanomaterials in multimodal imaging: Design, functionalization, and biomedical applications. *Journal of Nanomaterials*, *2010*, e894303. https://doi.org/10.1155/2010/894303

Lu, K., Goodwill, P. W., Saritas, E. U., Zheng, B., & Conolly, S. M. (2013). Linearity and shift invariance for quantitative magnetic particle imaging. *IEEE Transactions on Medical Imaging*, *32*(9), 1565–1575. https://doi.org/10.1109/TMI.2013.2257177

Ludewig, P., Gdaniec, N., Sedlacik, J., Forkert, N. D., Szwargulski, P., Graeser, M., Adam, G., Kaul, M. G., Krishnan, K. M., Ferguson, R. M., Khandhar, A. P., Walczak, P., Fiehler, J., Thomalla, G., Gerloff, C., Knopp, T., & Magnus, T. (2017). Magnetic particle imaging for real-time perfusion imaging in acute stroke. *ACS Nano*, *11*(10), 10480–10488. https://doi.org/10.1021/acsnano.7b05784

Ludewig, P., Sedlacik, J., Gelderblom, M., Bernreuther, C., Korkusuz, Y., Wagener, C., Gerloff, C., Fiehler, J., Magnus, T., & Horst, A. K. (2013). Carcinoembryonic Antigen–Related Cell Adhesion Molecule 1 Inhibits MMP-9–Mediated Blood–Brain–Barrier Breakdown in a Mouse Model for Ischemic Stroke. *Circulation Research*, *113*(8), 1013–1022. https://doi.org/10.1161/circresaha.113.301207

Macdougall, I. C., Strauss, W. E., McLaughlin, J., Li, Z., Dellanna, F., & Hertel, J. (2014). A randomized comparison of ferumoxytol and iron sucrose for treating iron deficiency anemia in patients with CKD. *Clinical Journal of the American Society of Nephrology: CJASN*, *9*(4), 705–712. https://doi.org/10.2215/CJN.05320513

Mason, E. E., Cooley, C. Z., Cauley, S. F., Griswold, M. A., Conolly, S. M., & Wald, L. L. (2017). Design analysis of an MPI human functional brain scanner. *International Journal on Magnetic Particle Imaging*, *3*(1). 1703008. https://doi.org/10.18416/ijmpi.2017.1703008

Meola, A., Rao, J., Chaudhary, N., Song, G., Zheng, X., & Chang, S. D. (2019). Magnetic particle imaging in neurosurgery. *World Neurosurgery*, *125*, 261–270. https://doi.org/10.1016/j.wneu.2019.01.180

Möddel, M., Griese, F., Kluth, T., & Knopp, T. (2020). Estimating orientation using multi-contrast MPI. *International Journal on Magnetic Particle Imaging*, *6*(2), 1–3. https://doi.org/10.18416/IJMPI.2020.2009023

Möddel, M., Meins, C., Dieckhoff, J., & Knopp, T. (2018). Viscosity quantification using multi-contrast magnetic particle imaging. *New Journal of Physics*, *20*(8), 83001. https://doi.org/10.1088/1367-2630/aad44b

Mohtashamdolatshahi, A., Kratz, H., Kosch, O., Hauptmann, R., Stolzenburg, N., Wiekhorst, F., Sack, I., Hamm, B., Taupitz, M., & Schnorr, J. (2020). In vivo magnetic particle imaging: Angiography of inferior vena cava and aorta in rats using newly developed multicore particles. *Scientific Reports*, *10*(1), 17247. https://doi.org/10.1038/s41598-020-74151-4

Molwitz, I., Ittrich, H., Knopp, T., Mummert, T., Salamon, J., Jung, C., Adam, G., & Kaul, M. G. (2019). First magnetic particle imaging angiography in human-sized organs by employing a multimodal ex vivo pig kidney perfusion system. *Physiological Measurement*, *40*(10), 105002. https://doi.org/10.1088/1361-6579/ab4436

Muslu, Y., Utkur, M., Demirel, O. B., & Saritas, E. U. (2018). Calibration-free relaxation-based multi-color magnetic particle imaging. *IEEE Transactions on Medical Imaging*, *37*(8), 1920–1931. https://doi.org/10.1109/TMI.2018.2818261

Nguyen, K.-L., Yoshida, T., Kathuria-Prakash, N. Zaki, I. H. Varallyay, C. G. Semple, S. I. & Saouaf, R. (2019). Multicenter Safety and Practice for Off-Label Diagnostic Use of Ferumoxytol in MRI. *Radiology*, *293*, 554–64. https://doi.org/10.1148/radiol.2019190477

Nothnagel, N., Rahmer, J., Gleich, B., Halkola, A., Buzug, T. M., & Borgert, J. (2016). Steering of magnetic devices with a magnetic particle imaging system. *IEEE Transactions on Biomedical Engineering*, *63*(11), 2286–2293. https://doi.org/10.1109/TBME.2016.2524070

Onishi, H., Murakami, T., Kim, T., Hori, M., Hirohashi, S., Matsuki, M., Narumi, Y., Imai, Y., Sakurai, K., & Nakamura, H. (2009). Safety of ferucarbotran in MR imaging of the liver: A pre- and postexamination questionnaire-based multicenter investigation. *Journal of Magnetic Resonance Imaging*, *29*(1), 106–111. https://doi.org/10.1002/jmri.21608

Orendorff, R., Peck, A. J., Zheng, B., Shirazi, S. N., Ferguson, R. M., Khandhar, A. P., Kemp, S. J., Goodwill, P., Krishnan, K. M., Brooks, G. A., Kaufer, D., & Conolly, S. (2017). First in-vivo traumatic brain injury imaging via magnetic particle imaging. *Physics in Medicine and Biology*, *62*(9), 3501–3509. https://doi.org/10.1088/1361-6560/aa52ad

P. Szwargulski, T. K., P. Ludewig, M. Graeser, M. Möddel, N. Gdaniec, K. M. Krishnan, H. Ittrich, G. Adam & T. Magnus (2018). Dynamic multi-colored magnetic particle imaging of a healthy mouse using multiple tracers. In World Molecular Imaging Congress (WMIC).

Petrov, V. N., & Ustinov, A. B. (2010). Magnetic properties of Fe3O4 surface. *Journal of Surface Investigation. X-ray, Synchrotron and Neutron Techniques*, *4*(3), 395–400. https://doi.org/10.1134/s1027451010030079

Rahmer, J., Halkola, A., Gleich, B., Schmale, I., & Borgert, J. (2015). First experimental evidence of the feasibility of multi-color magnetic particle imaging. *Physics in Medicine and Biology*, *60*(5), 1775–1791. https://doi.org/10.1088/0031-9155/60/5/1775

Rahmer, J., Wirtz, D., Bontus, C., Borgert, J., & Gleich, B. (2017). Interactive magnetic catheter steering with 3-D real-time feedback using multi-color magnetic particle imaging. *IEEE Transactions on Medical Imaging*, *36*(7), 1449–1456. https://doi.org/10.1109/TMI.2017.2679099

Rahmer, J., Stehning, C., & Gleich, B. (2017). Spatially selective remote magnetic actuation of identical helical micromachines. *Science Robotics*, *2*(3), eaal2845. https://doi.org/10.1126/scirobotics.aal2845

Rahmer, J., Stehning, C., & Gleich, B. (2018). Remote magnetic actuation using a clinical scale system. *PLoS One*, *13*(3), e0193546. https://doi.org/10.1371/journal.pone.0193546

Rahmer, J., Weizenecker, J., Gleich, B., & Borgert, J. (2009). Signal encoding in magnetic particle imaging: Properties of the system function. *BMC Medical Imaging*, *9*(4). https://doi.org/10.1186/1471-2342-9-4

Rauwerdink, A. M., Hansen, E. W., & Weaver, J. B. (2009). Nanoparticle temperature estimation in combined ac and dc magnetic fields. *Physics in Medicine and Biology*, *54*(19), L51–L55. https://doi.org/10.1088/0031-9155/54/19/L01

Rauwerdink, A. M., & Weaver, J. B. (2010a). Measurement of molecular binding using the Brownian motion of magnetic nanoparticle probes. *Applied Physics Letters*, *96*(3), 033702. https://doi.org/10.1063/1.3291063

Rauwerdink, A. M., & Weaver, J. B. (2010b). Viscous effects on nanoparticle magnetization harmonics. *Journal of Magnetism and Magnetic Materials*, *322*(6), 609–613. https://doi.org/10.1016/j.jmmm.2009.10.024

Reimer, P., & Balzer, T. (2003). Ferucarbotran (Resovist): a new clinically approved RES-specific contrast agent for contrast-enhanced MRI of the liver: properties, clinical development, and applications. *European Radiology*, *13*(6), 1266–1276. https://doi.org/10.1007/s00330-002-1721-7

Salamon, J., Dieckhoff, J., Kaul, M. G., Jung, C., Adam, G., Möddel, M., Knopp, T., Draack, S., Ludwig, F., & Ittrich, H. (2020). Visualization of spatial and temporal temperature distributions with magnetic particle imaging for liver tumor ablation therapy. *Scientific Reports*, *10*(1), https://doi.org/10.1038/s41598-020-64280-1

Saritas, E. U., Goodwill, P. W., & Conolly, S. M. (2015). Effects of pulse duration on magnetostimulation thresholds. *Medical Physics*, *42*(6), 3005–3012. https://doi.org/10.1118/1.4921209

Saritas, E. U., Goodwill, P. W., Zhang, G. Z., & Conolly, S. M. (2013). Magnetostimulation limits in magnetic particle imaging. *IEEE Transactions on Medical Imaging*, *32*(9), 1600–1610. https://doi.org/10.1109/TMI.2013.2260764

Sattel, T. F., Knopp, T., Biederer, S., Gleich, B., Weizenecker, J., Borgert, J., & Buzug, T. M. (2009). Single-sided device for magnetic particle imaging. *Journal of Physics D: Applied Physics*, *42*(2), 22001. https://doi.org/10.1088/0022-3727/42/2/022001

Saver, J. L. (2006). Time is brain—Quantified. *Stroke*, *37*(1), 263–266. https://doi.org/10.1161/01.STR.0000196957.55928.ab

Schiller, B., Bhat, P., & Sharma, A. (2014). Safety and effectiveness of ferumoxytol in hemodialysis patients at 3 dialysis chains in the United States over a 12-month period. *Clinical Therapeutics*, *36*(1), 70–83 https://doi.org/10.1016/j.clinthera.2013.09.028

Schmale, I., Borgert, B. G. J., & Weizenecker, J. (2010). Noise within magnetic particle imaging. In T. M. Buzug, J. Borgert, T. Knopp, S. Biederer, T. F. Sattel, M. Erbe, & K. Lüdtke-Buzug (Eds.), *Magnetic nanoparticles*. World Scientific Press. https://doi.org/10.1142/9789814324687_0022

Schmale, I., Gleich, B., Rahmer, J., Bontus, C., Schmidt, J., & Borgert, J. (2015). MPI safety in the view of MRI safety standards. *IEEE Transactions on Magnetics*, *51*(2), 6502604. https://doi.org/10.1109/TMAG.2014.2322940

Sehl, O. C., Gevaert, J. J., Melo, K. P., Knier, N. N., & Foster, P. J. (2020). A perspective on cell tracking with magnetic particle imaging. *Tomography*, *6*(4), 315–324. https://doi.org/10.18383/j.tom.2020.00043

Shasha, C., Teeman, E., & Krishnan, K. M. (2019). Nanoparticle core size optimization for magnetic particle imaging. *Biomedical Physics & Engineering Express*, *5*(5), 055010. https://doi.org/10.1088/2057-1976/ab3972

Song, G., Kenney, M., Chen, Y.-S., Zheng, X., Deng, Y., Chen, Z., Wang, S. X., Gambhir, S. S., Dai, H., & Rao, J. (2020). Carbon-coated FeCo nanoparticles as sensitive magnetic-particle-imaging tracers with photothermal and magnetothermal properties. *Nature Biomedical Engineering*, *4*(3), 325–334. https://doi.org/10.1038/s41551-019-0506-0

Srinivasan, A., Goyal, M., Lum, C., Nguyen, T., & Miller, W. (2005). Processing and interpretation times of CT angiogram and CT perfusion in stroke. *Canadian Journal of Neurological Sciences / Journal Canadien des Sciences Neurologiques*, *32*(4), 483–486. https://doi.org/10.1017/s0317167100004480

Stehning, C., Gleich, B., & Rahmer, J. (2016). Simultaneous magnetic particle imaging (MPI) and temperature mapping using multi-color MPI. *International Journal on Magnetic Particle Imaging*, *2*(6), 1–6. https://doi.org/10.18416/ijmpi.2016.1612001

Szwargulski, P., Ludewig, P., Graeser, M., Möddel, M., Gdaniec, N., Krishnan, K. M., Ittrich, H., Adam, G., Magnus, T., & Knopp, T. (2019). Dynamic multi-contrast imaging of two different tracer materials in a healthy mouse. In International Workshop on Magnetic Particle Imaging; pp. 97–98. https://submissions.infinite-science.de/index.php/iwmpi/article/view/120

Szwargulski, P., Ludewig, P., Wilmes, M., Javidi, E., Thieben, F., Graeser, M., Koch, M., Gruettner, C., Adam, G., Gerloff, C., Magnus, T., & Knopp, T. (2020). Monitoring intracranial cerebral hemorrhage using multicontrast real-time magnetic particle imaging. *ACS Nano*, *14*(10), 13913–13923. https://doi.org/10.1021/acsnano.0c06326

Theruvath, A. J., Aghighi, M., Iv, M., Nejadnik, H., Lavezo, J., Pisani, L. J., & Daldrup-Link, H. E. (2020). Brain iron deposition after Ferumoxytol-enhanced MRI: A study of Porcine Brains. *Nanotheranostics*, *4*(4), 195–200. https://doi.org/10.7150/ntno.46356

Tong, W., Hui, H., Shang, W., Zhang, Y., Tian, F., Ma, Q., Yang, X., Tian, J., & Chen, Y. (2021). Highly sensitive magnetic particle imaging of vulnerable atherosclerotic plaque with active myeloperoxidase-targeted nanoparticles. *Theranostics*, *11*(2), 506–521. https://doi.org/10.7150/thno.49812

US Food and Drug Administration. (2015). *FDA Drug Safety Communication: FDA strengthens warnings and changes prescribing instructions to decrease the risk of serious allergic reactions with anemia drug Feraheme (ferumoxytol)*. FDA. https://www.fda.gov/drugs/drug-safety-and-availability/fda-drug-safety-communication-fda-strengthens-warnings-and-changesprescribing-instructions-decrease

Utkur, M., Muslu, Y., & Saritas, E. U. (2019). Relaxation-based color magnetic particle imaging for viscosity mapping. *Applied Physics Letters*, *115*(15), 152403. https://doi.org/10.1063/1.5110475

Vaalma, S., Rahmer, J., Panagiotopoulos, N., Duschka, R. L., Borgert, J., Barkhausen, J., Vogt, F. M., & Haegele, J. (2017). Magnetic particle imaging (MPI): Experimental quantification of vascular stenosis using stationary stenosis phantoms. *PLoS One*, *12*(1), e0168902. https://doi.org/10.1371/journal.pone.0168902

Vadhan-Raj, S., Strauss, W., Ford, D., Bernard, K., Boccia, R., Li, J., & Allen, L. F. (2014). Efficacy and safety of IV ferumoxytol for adults with iron deficiency anemia previously unresponsive to or unable to tolerate oral iron. *American Journal of Hematology*, *89*(1), 7–12 https://doi.org/10.1002/ajh.23582

Vasanawala, S. S., Nguyen, K.-L., Hope, M. D., Bridges, M. D., Hope, T. A., Reeder, S. B., & Bashir, M. R. (2016). Safety and technique of ferumoxytol administration for MRI. *Magnetic Resonance in Medicine*, *75*(5), 2107–2111 https://doi.org/10.1002/mrm.26151

Viereck, T., Kuhlmann, C., Draack, S., Schilling, M., & Ludwig, F. (2017). Dual-frequency magnetic particle imaging of the Brownian particle contribution. *Journal of Magnetism and Magnetic Materials*, *427*, 156–161. https://doi.org/10.1016/j.jmmm.2016.11.003

Vogel, P., Ruckert, M. A., Kampf, T., Herz, S., Stang, A., Wockel, L., Bley, T. A., Dutz, S., & Behr, V. C. (2020). Superspeed bolus visualization for vascular magnetic particle imaging. *IEEE Transactions on Medical Imaging*, *39*(6), 2133–2139. https://doi.org/10.1109/tmi.2020.2965724

Vogel, P., Rückert, M. A., Kemp, S. J., Khandhar, A. P., Ferguson, R. M., Herz, S., Vilter, A., Klauer, P., Bley, T. A., & Krishnan, K. M. (2019). Micro-traveling wave magnetic particle imaging—Sub-millimeter resolution with optimized tracer LS-008. *IEEE Transactions on Magnetics*, *55*(10), 1–7. https://doi.org/10.1109/TMAG.2019.2924198

Vogel, P., Rückert, M. A., Klauer, P., Kullmann, W. H., Jakob, P. M., & Behr, V. C. (2014). Traveling wave magnetic particle imaging. *IEEE Transactions on Medical Imaging*, *33*(2), 400–407. https://doi.org/10.1109/tmi.2013.2285472

Vogel, P., Lother, S., Ruckert, M. A., Kullmann, W. H., Jakob, P. M., Fidler, F., & Behr, V. C. (2014). MRI meets MPI: A bimodal MPI-MRI tomograph. *IEEE Transactions on Medical Imaging*, *33*(10), 1954–1959. https://doi.org/10.1109/TMI.2014.2327515

Vogel, P., Markert, J., Rückert, M. A., Herz, S., Keßler, B., Dremel, K., Althoff, D., Weber, M., Buzug, T. M., Bley, T. A., Kullmann, W. H., Hanke, R., Zabler, S., & Behr, V. C. (2019). Magnetic particle imaging meets computed tomography: First simultaneous imaging. *Scientific Reports*, *9*(1), 12627. https://doi.org/10.1038/s41598-019-48960-1

Wang, Q., Ma, X., Liao, H., Liang, Z., Li, F., Tian, J., & Ling, D. (2020). Artificially engineered cubic iron oxide nanoparticle as a high-performance magnetic particle imaging tracer for stem cell tracking. *ACS Nano*, *14*(2), 2053–2062. https://doi.org/10.1021/acsnano.9b08660

Weaver, J. B., Rauwerdink, A. M., & Hansen, E. W. (2009). Magnetic nanoparticle temperature estimation. *Medical Physics*, *36*(5), 1822–1829. https://doi.org/10.1118/1.3106342

Weizenecker, J., Gleich, B., Rahmer, J., Dahnke, H., & Borgert, J. (2009). Three-dimensional real-time in vivo magnetic particle imaging. *Physics in Medicine and Biology*, *54*(5), L1–L10. https://doi.org/10.1088/0031-9155/54/5/L01

Weizenecker, J., Gleich, B., & Borgert, J. (2008). Magnetic particle imaging using a field free line. *Journal of Physics D: Applied Physics*, *41*(10), 105009. https://doi.org/10.1088/0022-3727/41/10/105009

Winder, A., d'Esterre, C. D., Menon, B. K., Fiehler, J., & Forkert, N. D. (2020). Automatic arterial input function selection in CT and MR perfusion datasets using deep convolutional neural networks. *Medical Physics*, *47*(9), 4199–4211. https://doi.org/10.1002/mp.14351

Wu, O., Østergaard, L., Weisskoff, R. M., Benner, T., Rosen, B. R., & Sorensen, A. G. (2003). Tracer arrival timing-insensitive technique for estimating flow in MR perfusion-weighted imaging using singular value decomposition with a block-circulant deconvolution matrix. *Magnetic Resonance in Medicine*, *50*(1), 164–174. https://doi.org/10.1002/mrm.10522

Yang, H.-W., Hua, M.-Y., Lin, K.-J., Wey, S.-P., Tsai, R.-Y., Wu, S.-Y., Lu, Y.-C., Liu, H.-L., Wu, T., & Ma, Y.-H. (2012). Bioconjugation of recombinant tissue plasminogen activator to magnetic nanocarriers for targeted thrombolysis. *International Journal of Nanomedicine*, *7*, 5159–5173. https://doi.org/10.2147/IJN.S32939

Zhao, Z., & Rinaldi, C. (2020). Computational predictions of enhanced magnetic particle imaging performance by magnetic nanoparticle chains. *Physics in Medicine and Biology*, *65*(18), 185013. https://doi.org/10.1088/1361-6560/ab95dd

Zheng, B., Vazin, T., Goodwill, P. W., Conway, A., Verma, A., Ulku Saritas, E., Schaffer, D., & Conolly, S. M. (2015). Magnetic particle imaging tracks the long-term fate of in vivo neural cell implants with high image contrast. *Scientific Reports*, *5*(1), 14055. https://doi.org/10.1038/srep14055

Ziemian, S., Löwa, N., Kosch, O., Bajj, D., Wiekhorst, F., & Schütz, G. (2018). Optimization of iron oxide tracer synthesis for magnetic particle imaging. *Nanomaterials*, *8*(4), 180. https://doi.org/10.3390/nano8040180

How to cite this article: Ludewig, P., Graeser, M., Forkert, N. D., Thieben, F., Rández-Garbayo, J., Rieckhoff, J., Lessmann, K., Förger, F., Szwargulski, P., Magnus, T., & Knopp, T. (2022). Magnetic particle imaging for assessment of cerebral perfusion and ischemia. *Wiley Interdisciplinary Reviews: Nanomedicine and Nanobiotechnology*, *14*(1), e1757. https://doi.org/10.1002/wnan.1757